People's Democratic Republic of Algeria
Ministry of Higher Education and Scientific Research
University M'Hamed BOUGARA – Boumerdes

Institute of Electrical and Electronic Engineering
Signals and Systems Research Laboratory

PHD DISSERTATION

PRESENTED BY:

Mustapha AMMICHE

IN PARTIAL FULFILMENT OF THE REQUIREMENTS FOR THE DEGREE OF

DOCTORATE

FIELD:ELECTRICAL ENGINEERING
OPTION:CONTROL, PROTECTION AND DIAGNOSIS OF SYSTEMS

TITLE:

Online Thresholding Techniques for Process Monitoring

JURY MEMBERS:

• Mr.	Kamel	HARICHE	*Prof*	University M'Hamed BOUGARA – Boumerdes, Algeria.	Jury president
• Mr.	Abdelmalek	KOUADRI	*MC-A*	University M'Hamed BOUGARA – Boumerdes, Algeria.	Thesis director
• Mr.	Ahmed	MAIDI	*Prof*	Mouloud MAAMERI University – Tizi Ouzou, Algeria.	Examiner
• Mr.	Hamid	BENTARZI	*Prof*	University M'Hamed BOUGARA – Boumerdes, Algeria.	Examiner

Academic year: 2017/2018

Abstract

Process monitoring via Principal Component Analysis (PCA) and Dynamic Principal Component Analysis (DPCA) suffer from the False Alarms (FAs), Missed Detection (MD) and to the Detection Time Delay (DTD). In this work, a Modified Moving Window PCA (MMWPCA) with Fuzzy Logic Filter (FLF) and its dynamic extension (MMW-DPCA) with FLF are proposed to overcome these issues. The techniques are based on PCA, DPCA and Moving Window PCA (MWPCA) to generate adaptive thresholds with fixed statistical models. The applications of the proposed methods have been carried out on the Tennessee Eastman Process (TEP) (both old and revised models), Photovoltaic system and cement rotary kiln. The performances of the developed techniques are compared against recent Fault Detection and Diagnosis (FDD) works. The results demonstrate the superiority of the proposed monitoring schemes in detecting different types of faults with high accuracy and with shorter time delay.

نبذة مختصرة

متابعة الأجهزة باستعمال تحليل المركبات الأساسية (PCA) و تحليل المركبات الأساسية الديناميكية (DPCA) تعاني من التنبؤ الكاذب، نقص وتأخر ال كشف. في هذا العمل، أقترح تعديل تحليل المركبات الأساسية ضمن نافذة متحركة (MMWPCA) مع الم رشح المنطقي الغامض (Fuzzy Logic Filter) و كذ لك النموذج الديناميكي (MMW-DPCA) لهذه التقنية لتغطية المشاكل المذكورة سابقا. هاتان التقنيتان تستندان على (PCA)، (DPCA) و النافذة المتحركة (PCA) لتوليد عتبات متكيفة مع نموذج إحصائي ثابت. هاتان الأخيرتان تم اختبارهما ومقارنة عملهما مع أعمال حديثة في مجال التقاط أعطاب الأجهزة و هذا بتطبيقهما على Tennessee Eastman Process (TEP) (الطراز الجديد والقديم) . كما أثبتت نجاعته ما في استشعار الخلل بدقة وفي وقت قصير على أجهزة واقعية مثل الألواح الشمسية و مصنع إنتاج الإسمنت.

Praise and glorification be only to Allah SWT, the Almighty, the most beneficent and the most merciful, whose blessing and guidance have helped us to finish this work.

I would like to express my sincere gratitude to my supervisor ***Dr. A. Kouadri*** for his inspirations, encouragement and guidance throughout this project.

My warm thanks to all IGEE family (students, teachers, workers) who all contributed in some way to this project.

Dedication

To my beloved parents,

To my brother "Abed El Halim"

To my two sisters "Zahra and Hayet",

To my uncle's family khoudir, Boualem. karim, Nabil, Anissa, Sakina,Razik, Souhila, Sabha, Malia, Noura,and their mother,

To my best friends

To those who will be happy for me.

Table Of Content

MSPC	Multivariate statistical Process Control	LGSSM	Linear Gaussian State Space Model
FDD	Fault Detection and Diagnosis	NR	Near Right
PCA	Principal Component Analysis	FR	FAR Right
DPCA	Dynamic PCA	XMEAS	Measured Variable
DPCA-DR)	Dynamic PCA with Decorrelated Residuals	XMV	Manipulated Variable
KPCA	Kernel PCA	CA	Canonical Analysis
EWPCA	Exponentially Weighted PCA	SLR	Switching Linear Regression
MWPCA	Moving Window (MWPCA)	MFDR	Mean Fault Detection Rate
EWMWPCA	Exponentially Weighted Moving Window PCA	PEARL	Power Electronic and Renewable Energy Research Laboratory
RPCA	Recursive PCA	INV	Inverter
AKPCA	Adaptive Kernel PCA	POLY	polycrystalline silicon
MWKPCA	Moving Window Kernel PCA	MONO	monocrystalline
DKPCA	Dynamic KPCA	PV	Photovoltaic
dpPCA	distributed and parallel PCA	NR	Near Left
LPPLS	Locality-Preserving Partial Least Squares	FL	Far Left
CPM	Constructive Polynomial Mapping	CPV	Cumulative Percentage Variance
LGSSM	Linear Gaussian State Space Model	CL	Confidence Level
CFAR	Constant False Alarms Rate	FA	False Alarms
MMWPCA	Modified Moving Window PCA	SMF	Standard Median Filter

FLF	Fuzzy Logic Filter	IMF	Improved Median Filter
MMW-DPCA	Modified Moving Window DPCA	SNR	Signal to Noise Ratio
TEP	Tennessee Eastman Process	LN	Large Negative
GCPVS	Grid-Connected Photovoltaic System	ST	Standard
FAR	False Alarms Rate	LP	Large Positive
MDR	Missed Detection Rate	SV	Short Value
DTD	Detection Time Delay	MV	Median Value
FDR	Fault Detection Rate	LV	Large Value
PCs	Principal Components	PLS	Partial Least Squares
ICA	Independent Canonical Analysis	CVA	Canonical Variante Analysis

Q	Square Predicted Error	d	Difference
T^2	Hotelling's statistic	B	Projection matrix
X_s	Scaled and shifted data matrix	X	Data matrix
$cov(X_s)$	Covariance matrix of X_s	S	Standard deviation
P	Orthonormal matrix of eigenvector	wn	Window of the proposed method
Λ	Diagonal matrix of eigenvalues	C_δ	Normal deviate
I	Identity matrix	$Cont$	Contribution
λ	Eigenvalue	e	Error
a	Number of PCs	k	Time Index
T	Score matrix	p	Eigen Vector
$\widehat{X_s}$	Estimated data matrix	$X_A(l)$	Augmented Data Matrix
E	Residual matrix	l	Number of Lags
x	Observation	H	Window Length
n	Total number of observations	T_δ^2	Control Limit for T^2
m	Number of Variables	CFARQ	CFAR monitoring index for Q
δ	Confidence value	$CFART^2$	CFAR monitoring index for T^2
Q_δ	Control Limit for Q	$CFARQ_{th}$	Control Limit for CFARQ
θ_i	Sum of eigenvalues in the residual Space	$CFART2_{th}$	Control Limit for $CFART^2$
V	Contains the Computed T^2	M	Mean
Q_{thin}	Initial Threshold for Q	W_i	Window
T^2_{thin}	Initial threshold for T^2	m_i	Median Value
Q_{fixed}	Fixed threshold for Q	r	Sample number
T^2_{fixed}	Fixed threshold for T^2	t	Time index
Q_f	Filtered Value of Q	f	Initial Filter Values
T^2_f	Filtered Value of T^2	Q_{fixed}	Adaptive Threshold for T^2
Q_{ad}	Adaptive Threshold for Q		
$\widehat{P}$	Matrix of PCs	$\widehat{\Lambda}$	Matrix of Principal eigenvalues
$\widetilde{P}$	Matrix of Residual Component	$\widetilde{\Lambda}$	Matrix of residual eigenvalues

Introduction

Introduction

Industrial product quality, production rate, performance efficiency and consumers demands satisfaction do not depend only on the high performance of the control systems but also on the efficient approaches of process monitoring. Industrial systems are subjected to malfunctions and faults which may lead to overall failures, fatal accidents, economic losses and environmental damages, thus process monitoring becomes a necessity to ensure safe and reliable operation of the entire system as well as to prevent the undesired consequences which faults may cause [1-11].

Literature Review

Multivariate Statistical Process Control (MSPC) techniques have been widely applied to monitor large-scaled data processes due to their ability of the dimensionality reduction [12-16]. Principal Component Analysis (PCA) is a well known MSPC technique that has been extensively used for the stated objective [17-18]. It is a projection method that maps the data onto a lower dimensional space by means of a linear transformation that accurately characterizes the process [17-28]. Processes are monitored via PCA using two control charts which reflect their status, the Hotelling's T^2 and Q statistics [19, 27, 29-30]. Regardless of how the fault control limits are developed, a fault is detected if either or both T^2 and Q violate their corresponding thresholds. PCA model does not include the dynamic behaviour of the data; hence it had been extended to the dynamic PCA by Ku et al [31]. Rato et al [32-33] noticed that the residuals of the DPCA show an auto-correlation. To handle this issue, they developed DPCA with Decorrelated Residuals (DPCA-DR) based on the generation of decorrelated residuals. The DPCA of Ku at al [31] adds the same number of lags to the process variables; however, a measured variable may need a number of lags that is different from the other variables. Thus, Rato at al [34] provided another methodology by which different numbers of lags are given to

the variables. Real processes are nonlinear; consequently, the measured data exhibit nonlinear behaviours which can be managed through the use of Kernel PCA (KPCA) by which a nonlinear transformation is employed instead of a linear one [35-43]. The operation set-points change is another problem which is added to the process monitoring using MSPC. To deal with this problem, several adaptive algorithms have been proposed in literature. For instance, Moving Window (MWPCA) [33, 44-45], fast MWPCA [46], Exponentially Weighted Moving Window PCA (EWMWPCA) [47] and Recursive PCA (RPCA) [48-49] are those PCA adaptive methods. Adaptive algorithms of KPCA, which are used to handle both nonlinear behaviours and the systems' changes in the operation conditions, include the Adaptive Kernel PCA (AKPCA) [50-51] and Moving Window Kernel PCA (MWKPCA) [52-53]. Combined methods such as Dynamic KPCA (DKPCA) have been developed to deal with both nonlinear and dynamic features of a process [11]. To enhance PCA in particular and its versions in general, many recent techniques were developed. For example, Zhu et al [21] developed distributed and parallel PCA (dpPCA) to monitor multivariate process, which divides a system onto several blocks. With this method, distribution and parallel analysis is performed then PCA is applied to extract features of each block. By considering all the PCA results, conclusions are made about the process status. Lou et al [54] proposed two step PCA to compact the dynamic behaviour in the steady states. Rato et al [55] used the Markovian and Non-Markovian sensitivity enhancing transformations which are applied to one of the PCA and DPCA monitoring index, T^2, to improve its sensitivity. Constructive Polynomial Mapping (CPM) has been used with DPCA and Linear Gaussian State Space Model (LGSSM) to address the problem of infinite order mapping of radial basis kernel function [56]. Other non based PCA techniques were used in fault detection and diagnosis. The most useful ones are the Partial Least Squares (PLS) [57], Canonical Variante Analysis (CVA) [58] and Independent Canonical Analysis (ICA) [59].

Motivation

Problem Statement and Objectives

The performance of any monitoring scheme depends on the quantified values of the False Alarms Rate (FAR), the Missed Detection Rate (MDR) and the Detection Time Delay (DTD) [60]. These criteria are required to be as small as possible [61]. The FAR, MDR and the DTD are dependent on each other, in other words, reducing one factor will increase the two other ones. PCA based fault detection method fails to fulfil the process monitoring performance requirements due to the assumptions under which its statistical model is constructed. For linear systems of few dynamics with independent observations and which do not exhibit the operation set-points changes, PCA shows high potential and good monitoring performance. However, with nowadays industrial processes, these assumptions become no longer valid. The application of PCA and its extended versions with fixed control limits to process monitoring delays the fault detection and results in high values of the FAR and MDR which worsen their performances. Consequently, the fault detection accuracy is decreased and the operators will confuse on what decision they must make. Even though the adaptive techniques generate adaptive thresholds for the monitoring indices, they suffer from the sensitivity to small amplitude faults owing to their model updating at each normal observation. Each one of the fault detection techniques has advantages and drawbacks; hence, a combination of different fault detection methods is a good solution to enhance process monitoring. The main objective of this work is to achieve early fault detection with high accuracy and less MDR. For that purpose, Constant False Alarms Rate (CFAR), a Modified Moving Window PCA (MMWPCA) with a Fuzzy Logic Filter (FLF) and its extension to Modified Moving Window

DPCA with FLF are proposed for online process monitoring. The CFAR method investigates in the number of false alarms to detect fault. This method is basically based on statistics, the CFAR is computed for PCA monitoring indices, and then a fault is detected whenever one or both CFARs exceed their corresponding limits. The MMWPCA with FLF combines the advantages of both PCA and conventional MWPCA techniques. The idea is to enhance PCA performance by means of adaptive thresholds and FLF. Both the adaptive thresholds and the FLF involve in the PCA monitoring indices sensitivity improvement, the FAR and MDR reduction. The FLF removes outliers and corrects any corrupted samples by noise in the Q and T^2. It is important to filter the monitoring indices before making decisions about the process status because false alarms are generated due to the existence of random noise and dynamic behaviours. Besides, the statistical formulas, by which the control limits are evaluated, always allow certain percentage of normal observations to exceed the thresholds. The control limits of the MMWPCA with FLF are updated only when a new normal observation is available. The MMW-DPCA with FLF is a dynamic version of the MMWPCA with FLF to include the dynamic behaviour in the statistical model.

The application of the proposed methods has been carried out on several processes. CFAR has been applied to the cement rotary kiln of Ain EL Kebira, Algeria. MMWPCA with FLF has been validated on the Tennessee Eastman Process (TEP) (both old and revised models). In addition, the real experimental applications of this method have been performed on the cement rotary kiln and on a photovoltaic system. MMW-DPCA with FLF has been applied to old TEP model. The results of the CFAR based fault detection demonstrate that the proposal scheme detect faults with high accuracy. The performance comparison of the MMWPCA and MMW-DPCA with FLF against some recently published papers in the field of FDD reveals the effectiveness of the developed adaptive thresholding schemes in detecting faults with reduced FAR, MDR and detection delay.

The rest of the thesis is organized as follows, chapter one provides some basics definitions and concepts in the field of fault detection and diagnosis. In chapter two, the well-known data-driven methods are presented and explained how they can be used to detect faults. The reviewed techniques are the PCA, DPCA and MWPCA. These methods are the platforms of the proposed monitoring schemes. Chapter three is devoted to the developed fault detection proposals where they are explained and their algorithms are offered. The applications of the CFAR, the MMWPCA and the MMW-DPCA with FLF are shown in chapter four. The obtained results are also discussed in this chapter. The findings, conclusions and future works are presented in the conclusion part.

Chapter One

Introduction to Fault Detection and Diagnosis

The basic definitions in the field of Fault Detection and Diagnosis (FDD) are provided in this chapter. The FDD approaches are also reviewed. Moreover, this chapter covers the quantified factors on which the monitoring performance analysis is based and their mathematical equations are given.

1. Introduction to Fault Detection and Diagnosis

1.1. Fault

Fault is an unaccepted deviation of at least one parameter, characteristic or property of the system from its normal behavior, usual and standard conditions [62-63].

1.1.1. Types of Faults

Regarding to the fault location in the system, faults can be classified as [64].

A) Actuator fault

B) Plant fault

C) Sensors fault

Figure 1.1 represents the different possible locations of a fault.

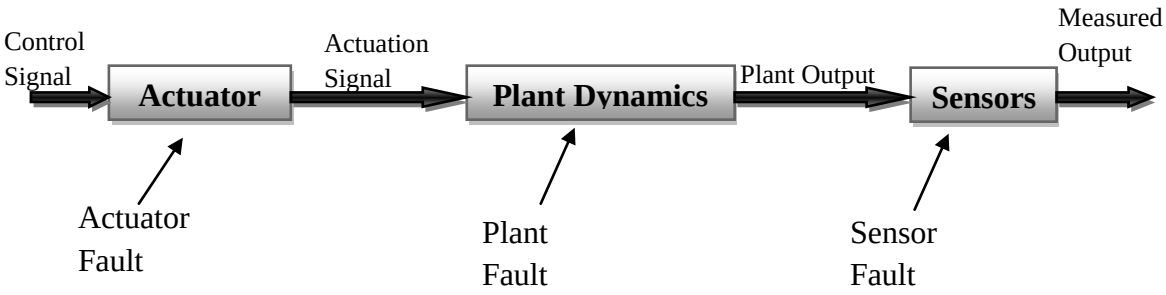

Figure 1.1. Possible locations of faults

A fault can be also classified according to the time behavior as [63]

D) Abrupt fault.

E) Intermittent fault

F) Incipient fault

Figure 1.2 represents the different types of faults according to the time behaviour.

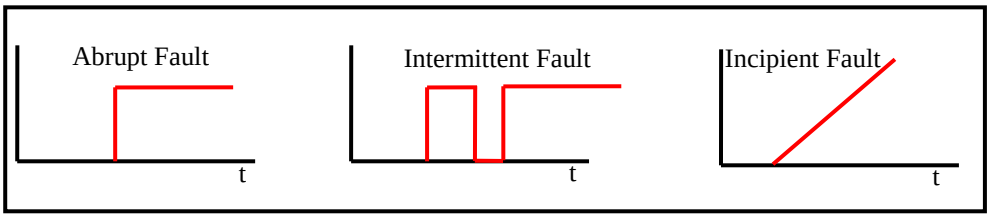

Figure 1.2. Time properties of a fault

1.2. Process Monitoring

The tasks which constitute the process monitoring are: the fault detection, fault identification, fault diagnosis and fault recovery [65]. Figure 1.3 represents the process monitoring loop.

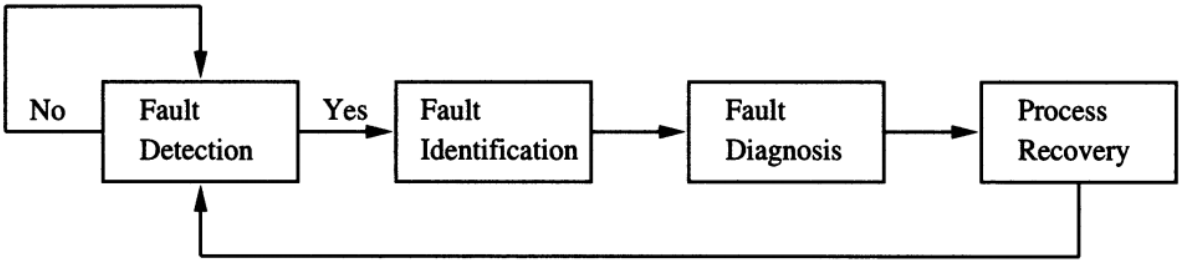

Figure 1.3. Process monitoring tasks

1.2.1. Fault Detection

Fault detection is the task which permits to determine whether an abnormal behavior has occurred [65].

1.2.2. Fault Identification

Fault identification is identifying the variable or variables which are responsible of the occurred fault [65]

1.2.3. Fault Diagnosis

Fault diagnosis is determining the type, location, amplitude and the time of the fault [65].

1.2.4. Process Recovery

Process recovery is removing the effect of the occurred fault [65].

1.3. Fault Detection and Diagnosis Approaches

Fault Detection and Diagnosis (FDD) approaches are classified in two major categories: the model-based and historical-based or data-driven. Both classes are divided into the qualitative and quantitative techniques. Statistic and neural network constitute the quantitative data-driven while the qualitative data-driven is consisted of the expert system and Qualitative trend Analysis (QTA). The qualitative model-based is divided into the causal models and abstraction hierarchy methods. The use of mathematical functions classifies the quantitative model-based [66-68]. The Fault detection and diagnosis tree is depicted in Figure 1.4.

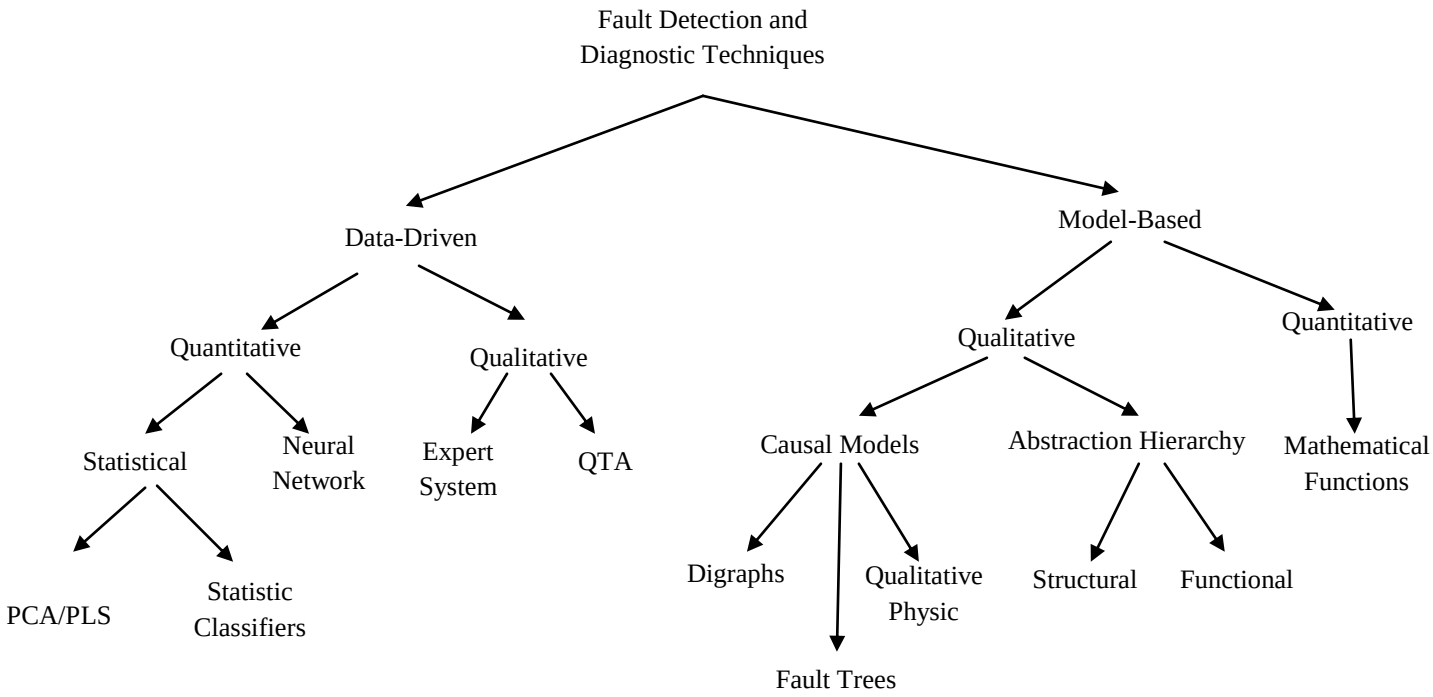

Figure 1.4. FDD approaches

1.3.1. Model-Based Fault Detection Techniques

1.3.1.1. Quantitative Methods

Quantitative methods use the relationships between the inputs and the outputs of the systems. These relationships are expressed through mathematical functions based on the knowledge of physics of the process in the form of differential or state space equations. The process monitoring via this class of model-based is performed by the residuals generation techniques such as nonlinear observer –based residual generation that has been extensively applied [66-67].

1.3.1.2. Qualitative Methods

Qualitative methods also use the relationships between the inputs and the outputs of the system. However, with these techniques, the relationships are expressed in terms of qualitative functions which are either causal models or abstraction hierarchies [67].

1.3.1.2.1. Causal Methods

Causal methods can be achieved by signed direct graphs, fault tree or qualitative physic. **Signed Direct Graph (SDG)**, which can be derived from differential equations for the process [67, 69], is a graph that reflects the behavior of the equipments and the general process behavior. In SDG, the cause-effect relations can be represented. High and low thresholds for the process variables are first defined then a node takes the value 0 when the measured value of a variable is in its normal conditions and takes positive value when the measured variable exceed the thresholds, otherwise it takes a negative value [65]. **Fault Tree** represents the relation between the fault and its symptoms [65]. A general fault tree analysis consists of the system definition, fault tree construction, qualitative evaluation and

quantitative evaluation [67]. By taking the intersection of the fault causes and the symptoms, the root cause of the fault is identified. **Qualitative physics** permits to draw conclusions about the systems status with incomplete knowledge of the physical process [70]. Two approaches are used with this method. The first is to derive qualitative equations from the differential equations as confluence equations. The second approach is to derive the qualitative behaviors from the differential equations which describe the system. These behaviors are then considered for fault detection and diagnosis [67,70].

1.3.1.2.2. Abstraction Hierarchy

Abstraction hierarchy is based on the decomposition which permits to draw inferences about the behavior of the process only from laws governing the behavior of its subsystems. But the laws of the subsystems may not reflect the functioning of the whole system. In a hierarchic presentation, a class of the process units can be presented and the equations describing the entire class may make assumptions about the class as a whole but not about the behavior of specific units [67]. Structural and functional decompositions are the most used in abstraction and hierarchy qualitative model-based methods. **Structural** defines the connectivity information of a unit while **functional** describes the unit's output as a function of its input [67].

The main drawback of the model-based fault detection approaches is their explicit dependency on the exact mathematical model of the process. The derivation of such model is a very challenging task to do for sophisticated and large- scaled systems.

1.3.2. Data-Driven Techniques

1.3.2.1. Qualitative Methods

Qualitative methods are divided into the expert system and trend analysis techniques. **An expert system** tends to solve problems in a narrow domain of expertise. The advantages of an

expert system in fault detection and diagnosis are: it is simple to develop, transparent in reasoning, able to provide explanation about the solution and its ability to reason under uncertainty. **Trend analysis** is another qualitative feature extraction technique. It is able to explain the various vital events occurring in the system to diagnose the malfunctions and to predict of the process states [68].

1.3.2.2. Quantitative Methods

Quantitative methods consist of statistical and neural network techniques. **Statistical** quantitative technique achieves fault detection and diagnosis by means of the use of statistical theories while fault detection via quantitative **neural network** is accomplished via neural networks approaches [68].

Modern industrial systems are sophisticated, complex and large-scaled data for which an exact mathematical model is difficult to be obtained [71-73]. However, such processes, with the development of the data acquisition, provide large amount of data that can be exploited to extract information about their operation status. This feature gives the data-driven techniques a priority and an advantage to monitor modern processes because only measurements are required [65, 68, 72, 74].

1.4. Multivariate Statistical Process Control

Multivariate is an extension of the univariate Shewhart, Cumulative Sum (CUSUM) and Exponentially Weighted Moving Average (EWMA) control charts [75]. Univariate charts provide efficient information when monitoring an individual characteristic but they become less efficient when monitoring processes with large-scaled data [76]. Multivariate Statistical Process Control (MSPC) techniques address some limitations of the univariate monitoring methods by extracting information based on the variations of the whole data simultaneously

[20, 77-78]. Multivariate statistical projections combined with monitoring charts are widely used for dimensionality reduction and fault detection [30].

1.5. Monitoring Scheme Performance Analysis

The performance analysis of any monitoring scheme is based on the quantified values of the False Alarms rate (FAR), the Missed Detection Rate (MDR) and the Detection Time Delay (DTD). The more these values are reduced, the more efficient the monitoring scheme is [60-61]. **FAR** returns the rate of the normal samples detected as faulty samples. In statistics, the FAR corresponds to the type I error of the evaluated statistical control chart. The FAR can computed using the following equation

$$FAR = \frac{Number\ \ of\ normal\ \ samples\ \ above\ \ the\ limits}{total\ \ number\ \ of\ normal\ \ samples} * 100 \quad (1.1)$$

The **MDR** represents the rate of non detected faulty samples. It is given by

$$MDR = \frac{Number\ \ of\ faulty\ \ samples\ \ under\ \ the\ limits}{total\ \ number\ \ of\ faulty\ \ samples} * 100 \quad (1.2)$$

The **DTD** is provided as

$$DTD = fault\ detection\ time - fault\ occurrence\ time \quad (1.3)$$

Fault Detection Rate (FDR) is another criterion used to evaluate the performance of a monitoring scheme. It measures the rate of the detected samples over the total number of faulty samples. It can be calculated using the Eq. (1.4)

$$FDR = \frac{Numberoffaulty\ \ \ samples\ \ above\ \ the\ limits}{total\ \ number\ \ of\ faulty\ \ samples} * 100 \quad (1.4)$$

The FDD concepts have been given in this chapter. These definitions provide a general overview of the FDD. The necessary tasks of process monitoring and the different approaches

of FDD are reviewed also in this chapter. In the next chapter, the well-known data-driven methods will be presented and explained.

Chapter Two

Data-Driven Techniques

The Principal Component Analysis (PCA), Dynamic PCA (DPCA) and the conventional MWPCA are reviewed in this chapter. These well-known data-driven techniques are the basics of the proposed monitoring schemes which are provided in chapter three. The definitions of these methods and their mathematical formulations are presented. In addition, their application to the process monitoring is also discussed throughout this chapter.

2. Data-Driven Techniques

2.1. Principal Component Analysis

2.1.1. Definition and Mathematical formulation

Principal Component Analysis (PCA) is widely used for dimensionality reduction of large-scaled data processes. It projects the original correlated data onto a lower dimensional uncorrelated data while preserving as much as possible the carried variability on the original variables. PCA based fault detection is performed by monitoring the principal component and the residual subspaces which are defined after the determination of the Principal Components (PCs) [79-89]. A data-set of m measured variables and n observations, collected from an ergodic process, is stored in the matrix $X \in R^{n\times m}$ that is defined as follows

$$X = \begin{pmatrix} x_{11} & x_{12} & \cdots & x_{1m} \\ x_{21} & x_{22} & \cdots & x_{2m} \\ \vdots & \vdots & \vdots & \vdots \\ x_{n1} & x_{n2} & \dots & x_{nm} \end{pmatrix} \tag{2.1}$$

Since the process variables are measured with different units and scales, it is necessary to scale and shift the matrix X to zero mean and unity variance by means of the mean $M \in R^{1\times m}$ and the standard deviation $S \in R^{1\times m}$ of the matrix X. Let X_s be the scaled and shifted data matrix. The uncorrelated data are given by the score matrix $T \in R^{n\times m}$ that defines the projection. This matrix is provided by

$$T = X_s P \tag{2.2}$$

In which $P \in R^{m \times m}$ is a matrix of the eigenvectors of the covariance matrix of X_s that satisfies $PP^T = I$. This matrix is determined through the Eigen Value Decomposition (EVD) of the covariance matrix.

$$cov(X_s) = P^T \Lambda P \tag{2.3}$$

$\Lambda \in R^{m \times m}$ is a diagonal matrix where the diagonal elements are the eigenvalues of the covariance matrix.

2.1.2. Number of Retained Principal Components

The PCA model depends on the number of Principal Components (PCs), *a*, to be retained. A large value of *a* includes noise in the model and a small value of *a* deteriorates the process description by the model [65]. In literature, many criteria are utilized for the number of PCs, *a* selection [65, 85, 90]. The employed techniques, in this work, are the parallel analysis, Cumulative Percentage Variance (CPV) and Kaiser's rule.

A. Parallel Analysis

The number of PCs by the parallel analysis criterion is defined as the cross point of the eigenvalues profile of the original data and the eigenvalues profile of generated data assuming independent observations [65].

B. Cumulative Percentage Variance

Cumulative Percentage Variance (CPV) picks up the PCs associated with a percentage of variance less or equal to a predefined value. CPV is generally set between 90% and 95%. CPV is given as [65, 90]

$$CPV(a) = \frac{\sum_{j=1}^{a} \lambda_j}{\sum_{i=1}^{m} \lambda_i} 100\% \tag{2.4}$$

C. Kaiser's Rule

Kaiser's rule retains all the principal components which correspond to the eigenvalues greater than one [91-92].

The number of PCs allows the definition of two subspaces, the principal component subspace spanned by the first *a* eigenvectors and the residual subspace that is spanned by the *m-a* eigenvectors. The T , Λ and P matrices are decomposed as

$$T = \left(\hat{T}\middle|\tilde{T}\right) \tag{2.5}$$

$$P = \left(\hat{\mathrm{P}}\middle|\tilde{\mathrm{P}}\right) \tag{2.6}$$

$$\Lambda = \begin{pmatrix} \hat{\Lambda} & 0 \\ 0 & \tilde{\Lambda} \end{pmatrix} \tag{2.7}$$

Where $\hat{\mathrm{T}} \in R^{n\times a}$ and $\tilde{\mathrm{T}} \in R^{n\times(m-a)}$. $\hat{\mathrm{P}} \in R^{mxa}$ and $\tilde{\mathrm{P}} \in R^{mx\,(m-a)}$. $\hat{\Lambda} \in R^{a\times a}$ and $\tilde{\Lambda} \in R^{(m-a)\times(m-a)}$.

Eq. (2.2) permits to rewrite the matrix X_s as follows

$$X_s = TP^T \tag{2.8}$$

$$X_s = \hat{T}\hat{P}^T + \tilde{T}\tilde{P}^T \tag{2.9}$$

$\hat{T}\hat{P}^T$ is the estimated data matrix $\hat{X}_s$ whereas $\tilde{T}\tilde{P}^T$ is the residual matrix.

2.1.3. Monitoring Indices

PCA based fault detection is characterized by two different monitoring indices the Hotelling's T^2 [93] and Q [94]. The T^2 measures how far the observation is from the origin while the Q measures how good the PCA model is. The Q statistic is the Square Predicted

Error (SPE). For each monitoring index, a threshold is determined. T^2 and Q with their thresholds are given by the Eq. (2.10), (2.11), (2.12) and (2.13).

$$T^2 = x\hat{\mathrm{P}}\hat{\Lambda}^{-1}\hat{\mathrm{P}}^{\mathrm{T}}x^T \tag{2.10}$$

$$Q = \left\|(I - \hat{\mathrm{P}}\hat{\mathrm{P}}^{\mathrm{T}})x^T\right\|^2 = x\,(I - \hat{\mathrm{P}}\hat{\mathrm{P}}^{\mathrm{T}})^2x^T \tag{2.11}$$

$$T_\delta^2 = \frac{a(n-1)(n+1)}{n(n-a)}F_\delta(a, n-a) \tag{2.12}$$

$$Q_\delta = \theta_1\left(\frac{C_\delta\sqrt{2\theta_2h_0^2}}{\theta_1} + 1 + \frac{\theta_2h_0(h_0-1)}{\theta_1^2}\right)^{\frac{1}{h_0}} \tag{2.13}$$

Where $F_\delta(a, n-a)$ is the upper δ percentile of an F-distribution with *a*, *n-a* degree.

C_δ is the normal deviate corresponding to $(1-\delta)$ percentile.

$$\theta_i = \sum_{j=a+1}^{m}\lambda_{\mathrm{j}}^{\mathrm{i}} \quad , \quad \mathrm{i} = 1,2,3 \tag{2.14}$$

$$h_0 = 1 - \frac{2\theta_1\theta_2}{3\theta_2^2} \tag{2.15}$$

2.1.4. Fault Detection Using PCA

If one or both of the monitoring indices exceed their associated threshold, then a fault is detected. As it is mentioned previously, the monitoring indices measure the variations in different subspaces; hence, it is preferable to use both of them when monitoring a process.

The PCA algorithm for fault detection is provided by the following phases

A. Offline Phase

1. Construct the PCA model (the mean, standard deviation and the number of PCs) using the training data-set.
2. Compute the monitoring indices for the samples of the training data-set.
3. Evaluate the thresholds for a given Confidence Level (CL), δ.

B. Online Phase

1. Get the new testing sample.
2. Compute its monitoring indices using the constructed model.
3. Compare these monitoring indices with the specified thresholds. If both of them are less than their corresponding control limit, go to step 4 else go to step 5.
4. Generate no fault alarm and then repeat from 1.
5. Generate a fault alarm and then repeat from 1.

The offline phase is used to construct and validate the PCA model while the online phase is used to monitor the new testing samples. The flowchart of the algorithm is shown in the Figure 2.1.

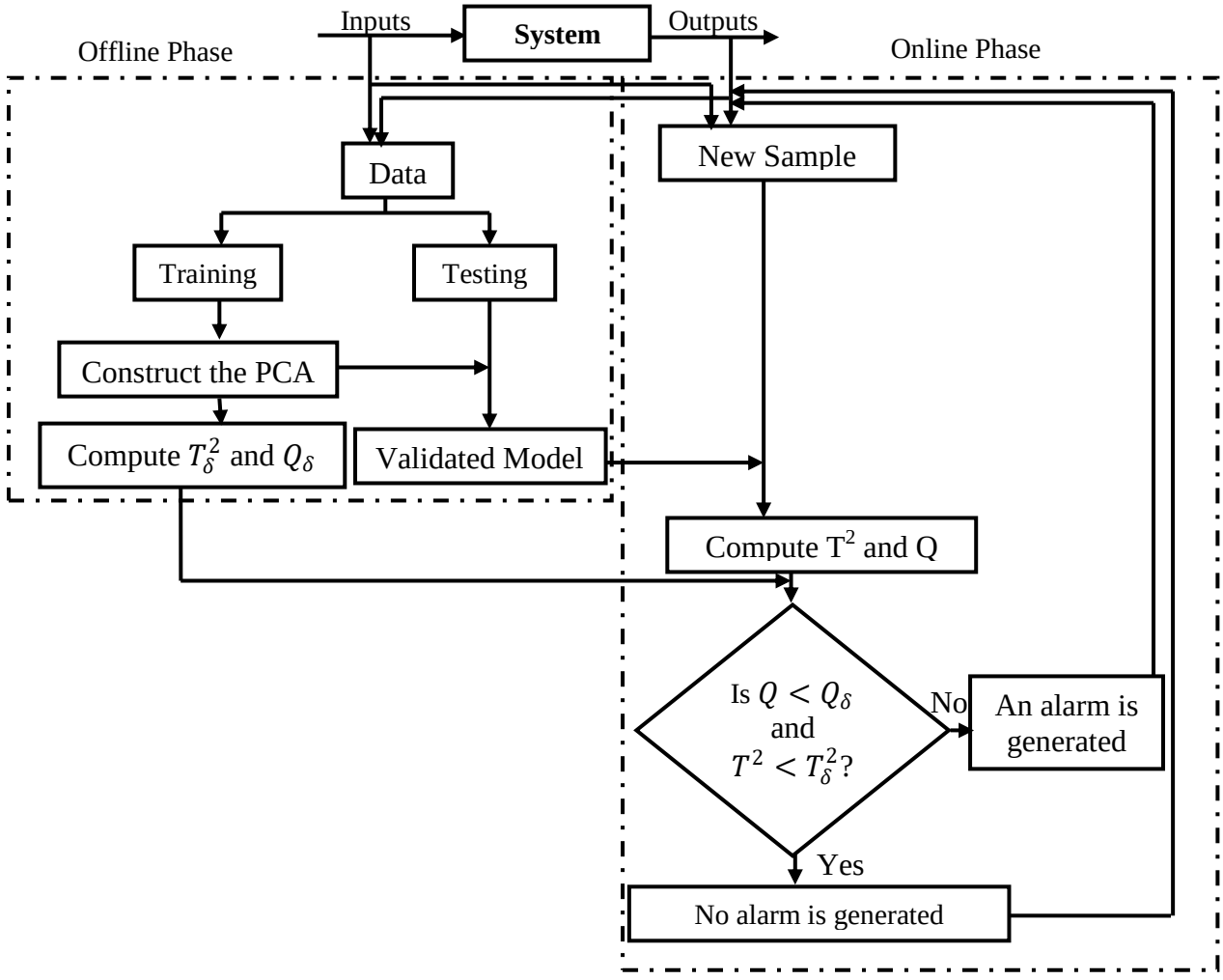

Figure 2.1. Flowchart of PCA

2.1.5. Fault Identification Using PCA

The fault identification via PCA is performed by determining the variables which mostly contribute to the monitoring indices [65]. The contribution of the j^{th} process variable to the Q statistic at the time period, k, is given by

$$Cont_j^Q(k) = \left(e_j(k)\right)^2 = \left(x_j(k) - \hat{x}_j(k)\right)^2 \quad (2.16)$$

In the case of T^2, the contribution of the j^{th} process variable is given by

$$Cont_{i,j}^{T^2}(k) = \frac{t_i(k)}{\lambda_i} p_{i,j}\, x_j(k) \quad (2.17)$$

Where $p_{i,j}$ is the j^{th} element of the eigenvector P_i corresponding to the eigenvalue λ_i and t_i is the i^{th} element (i=1...a) from the k^{th} row of the score matrix. $x_j(k)$ is the variable of the current observation. $Cont_{i,j}^{T^2}(k)$ is set to 0 if it is negative. The total contribution to the T^2 of the variable $x_j(k)$ is provided by:

$$CONT_j^{T^2}(k) = \sum_{i=1}^{a} Cont_{i,j}^{T^2}(k) \quad (2.18)$$

$Cont_j^Q$ and $CONT_j^{T^2}$ are plotted to provide good interpretation of the variables contribution. A variable with a high contribution value is identified as the fault source.

2.2. Dynamic Principal Component Analysis

Data measurements, form fast industrial processes, need a small sampling period to provide early fault detection. The statistical independency assumption between observations becomes no longer valid with small sampling interval; hence, the PCA performance will not satisfy the process monitoring requirements [58]. To include the dynamics of the data in the PCA model, Ku et al [31] extended PCA to Dynamic PCA (DPCA) through the use of the

time lag shift method. The current values of the process variables depend on the past values with the DPCA. The DPCA model is obtained by adding a necessary number of lags, *l*, to the data. If *l* is determined then, the augmented data matrix is

$$X_A(l) = \left(\begin{array}{cccc|cccc|c|cccc} x_{11} & x_{21} & \cdots & x_{(l+1)1} & x_{12} & x_{22} & \cdots & x_{(l+1)2} & \cdots & x_{1m} & x_{2m} & \cdots & x_{(l+1)m} \\ x_{21} & x_{31} & \cdots & x_{(l+2)1} & x_{22} & x_{32} & \cdots & x_{(l+2)2} & \cdots & x_{2m} & x_{3m} & \cdots & x_{(l+2)m} \\ \vdots & \vdots & \vdots & \vdots & \vdots & \vdots & \vdots & \vdots & \vdots & \vdots & \vdots & \vdots & \vdots \\ x_{(n-l)1} & x_{(n-l+1)1} & \cdots & x_{n1} & x_{(n-l)2} & x_{(n-l+1)2} & \cdots & x_{n2} & \cdots & x_{(n-l)m} & x_{(n-l+1)m} & \cdots & x_{nm} \end{array}\right) \quad (2.19)$$

Applying PCA to $X_A(l)$ allows the construction of the DPCA model. The monitoring procedures of the DPCA are the same as the ones of PCA. The main key of the DPCA is the number of lags to be selected. A lag will be included if it adds an important linear relationship for one of the variables [44]. Ku et al [31] provided algorithms to determine the required number of lags *l*. These methods select the same number of lags for all the process variables. These algorithms are well explained in Ku et al [31]. The dynamic relationship between the current and the past values of the process variables may differ from one variable to another. Based on this statement, Rato et al [34] developed an algorithm able to select necessary number of lags for each process variable. Rato et al [32-33] noticed that when the DPCA is applied to a process, the monitoring index Q still shows an auto-correlation. To handle this problem, they proposed DPCA with Decorrelated Residuals (DPCA-DR). This method handles also the serial correlation in the data.

2. 3. Conventional Moving Window Principal Component Analysis

The existence of dynamics in the industrial processes is not the only problem that is faced in process monitoring. Although the DPCA provides a dynamic statistical model, it fails to fulfill the fault detection requirements when it is applied to systems which exhibit operation set-points changes. To overcome this problem, researchers designed a multivariate statistical

technique able to track the system's changes. This method is the conventional Moving Window PCA (MWPCA). The systems changes are tracked by this method via the PCA model adaption. The monitoring indices thresholds of the MWPCA are adaptive allowing the FAR, and the MDR reduction in some cases. At each new normal observation, the PCA model is recalculated allowing the generation of the adaptive thresholds after the newest normal observation inclusion in the moving window and the oldest sample exclusion. For a window of size H, the data matrix is given at the time *t* as [33, 44-45]

$$X_t = (x_{t-H+1}, x_{t-H+2}, \dots x_t\ )^T \tag{2.20}$$

and at the time *t+1* as:

$$X_{t+1} = (x_{t-H+2}, x_{t-H+3}, \dots x_{t+1}\ )^T \tag{2.21}$$

The initial PCA model is constructed based on the training data-set and validated on the testing data-set.

The algorithm of the conventional MWPCA can be summarized in the following steps

A. Offline phase

1. Establish the initial PCA model based on training data (initialize the loading vectors, number of principal components and control limits of the monitoring indices, T^2 and Q statistics).
2. Validate the constructed model using a testing data-set.

B. Online Phase

1. Obtain the next testing sample x. Scale it using the current mean and standard deviation.
3. compute the monitoring indices for this observation
4. Compare the monitoring indices with the current thresholds. If both of them are under the thresholds, go to step 5, else go to step 6.

5. Include the sample in the moving window and exclude the oldest ones. Recalculate the PCA model and the thresholds. Repeat from step 1.
6. Generate an alarm. Go to step 1.

Figure 2.2 represents the flowchart of the conventional MWPCA.

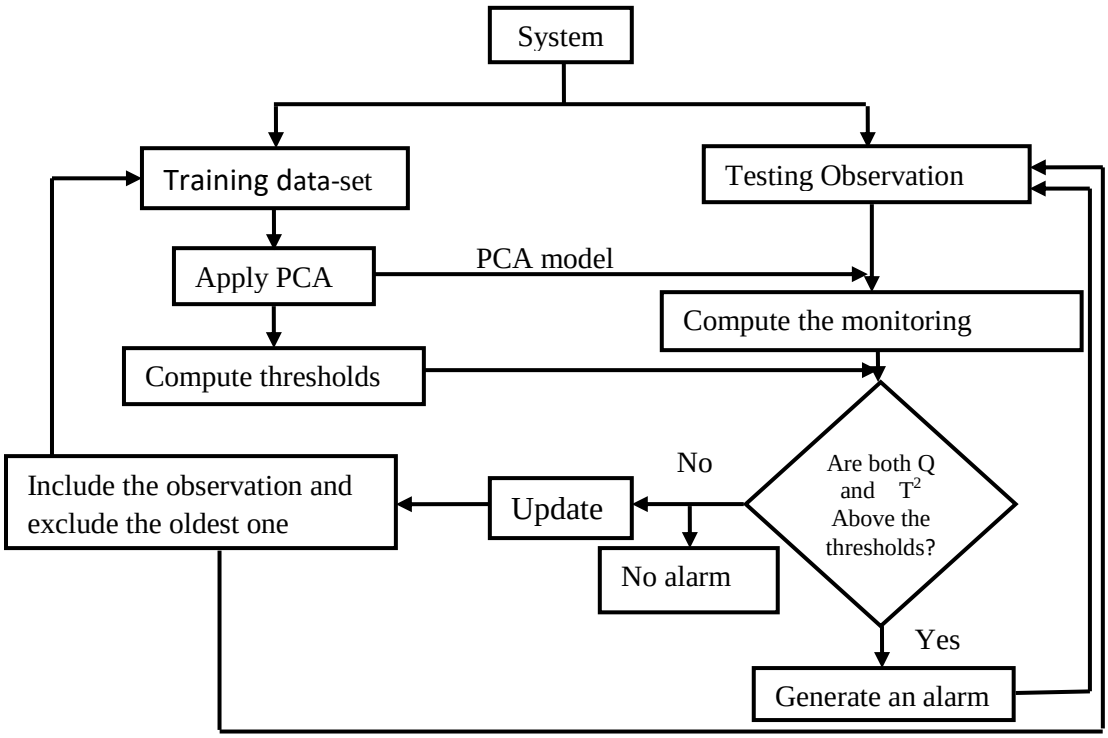

Figure 2.2. Flowchart of MWPCA

The well-known multivariate statistical process control techniques, PCA, MWPCA and DPCA, are reviewed and discussed. In addition, their mathematical formulations are provided. Furthermore, the use of these methods in fault detection is explained throughout the given algorithms and flowcharts. Since each one of the reviewed methods has advantages and disadvantages, a combined method will be a good solution to enhance and improve the data-driven techniques in process monitoring. In the next chapter, combined methods of MWPCA with PCA and DPCA are presented and explained how they enhance the performance of PCA, DPCA and MWPCA based fault detection schemes.

Chapter Three

Proposed Monitoring Schemes

In this chapter, three proposed methods are discussed. The Constant False Alarms Rate (CFAR) [95], the Modified Moving Window PCA (MMWPCA) with Fuzzy Logic Filter (FLF) [96-99] and the Modified Moving Window Dynamic PCA (MMW-DPCA) with FLF [100]. These methods are designed to reduce the FAR, MDR and the detection time delay. Mainly, two solutions are presented by the methods. The first one is to investigate in the number of false alarms; this solution corresponds to the CFAR technique. The second one is to monitor processes with adaptive thresholds combined with filters.

3. Proposed Monitoring Schemes

3.1. Constant False Alarms Rate

The mathematical formulas used to develop the control limits of the PCA monitoring indices allow a certain number of normal samples to exceed the thresholds. This percentage is associated with type I error. It is also evident that when a fault is occurs, the number of samples above the thresholds is increased; thus, the idea behind the Constant False Alarms Rate (CFAR) is to detect faults through the number of samples which violate the PCA control limits [95]. To do so, PCA method is applied to the training data-set in order to determine a descriptive statistical model of the process with the fixed thresholds. Through the offline phase, a window of fixed length is sliding over the obtained monitoring indices vectors (Q and T^2) where the number of sample above the control limits is computed at each iteration. The obtained numbers for each monitoring index are stored in vectors which will be used to compute empirically the CFAR thresholds by estimating their distributions. At the end of the offline phase, two CFAR thresholds are obtained, the $CFARQ_{th}$ and the $CFART^2_{th}$ associated with the computed CFARQ and $CFART^2$ indices. The CFAR is provided as [95]

$$CFAR(i) = \frac{Number\ \ of\ samples\ \ above\ \ the\ limits}{Window\ \ lengt\ h} * 100 \qquad (3.1)$$

In the online phase, the monitoring indices of the new testing sample are calculated using the constructed PCA model. These monitoring indices are then included in the moving window after removing the oldest observation indices. Within the updated window, the number of samples above the fixed PCA thresholds is computed and compared against the predefined CFAR thresholds. If both CFARQ and $CFART^2$ are greater than their corresponding CFAR thresholds, then a fault alarm is generated otherwise, the sample is considered to be normal. Figure 3.1 summarizes the different steps of the CFAR algorithm.

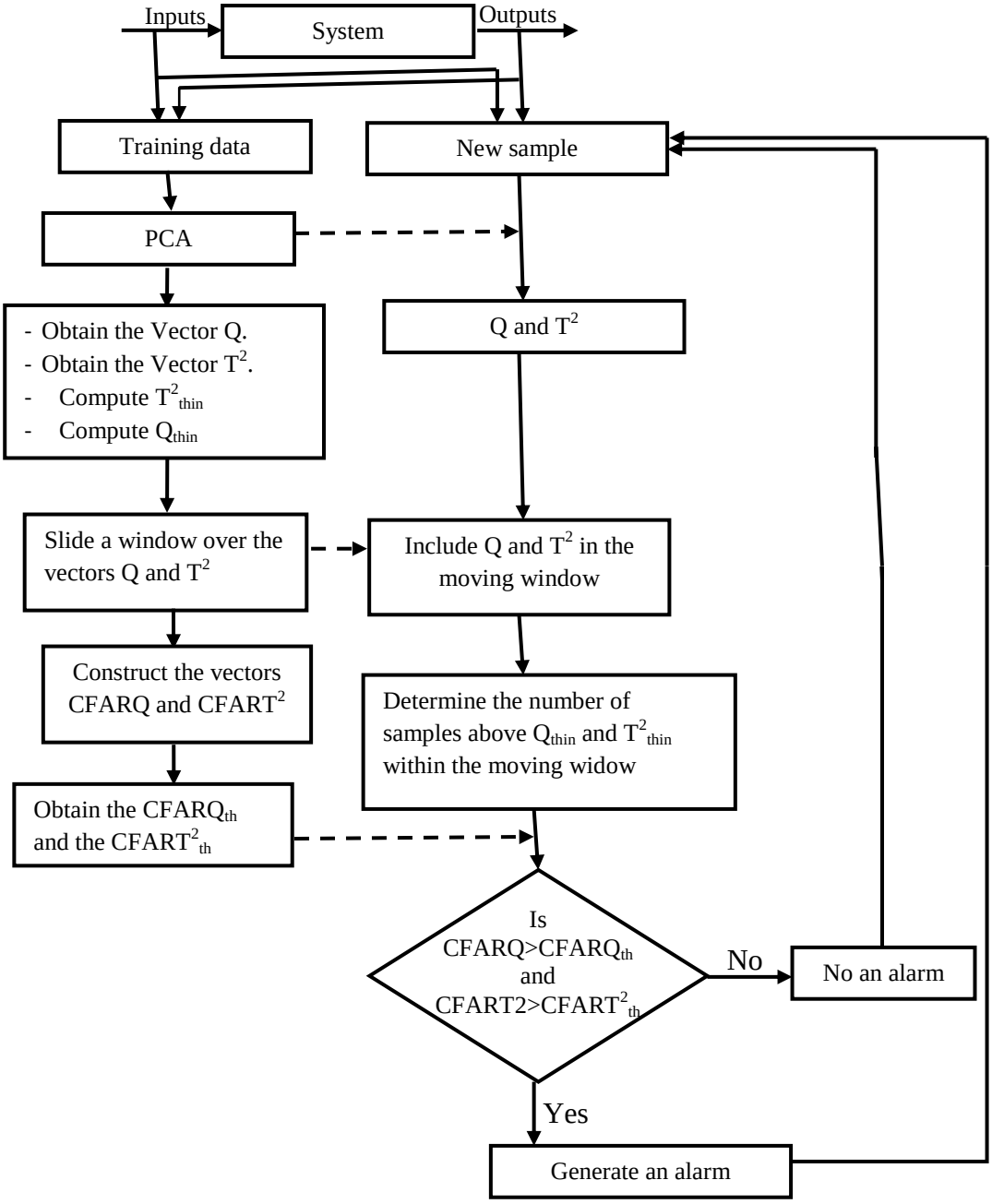

Figure 3.1. Flowchart of the CFAR method

The CFAR thresholds are determined empirically by estimating the distributions of the vectors CFARQ and CFART^2 in the offline phase.

3.2. Modified Moving Window PCA with Fuzzy Logic Filter

Modified Moving Window PCA (MMWPCA) with Fuzzy Logic Filter (FLF) is a data-driven method combined with FLF. This technique is based on the two well-known MSPC approaches, PCA and MWPCA. The PCA technique allows the construction of a model that will evaluate the monitoring indices of each new testing sample while the MWPCA permits the generation of the adaptive thresholds which will enhance the PCA monitoring indices sensitivity, robustness and will decrease the MDR. The FLF filters the evaluated monitoring indices to reduce both the FAR and MDR. In addition, it makes the whole proposed scheme robust to noise and outliers [96-99].

3.2.1. Fuzzy Logic Filter

Filters have been widely used to remove noise and outliers from different signals for a variety of applications. In literature, plenty of filters types have been implemented [101-102]. The design of a filter for fault detection applications must take the filtering action effects on monitoring. The implemented filter must not affect too much the monitoring indices sensitivity of the used FD method. Three types of filter have been analyzed, using the rotary kiln data described in the next chapter, before the FLF is implemented. These filters are, the Standard Median Filter (SMF), the Improved Median Filter (IMF) and the fuzzy based filter. The filters effect on process monitoring via PCA has been studied based on the FARs and the Signal to Noise Ratio (SNR) recorded for the Q and T^2 monitoring indices [103]. The SNR is given by

$$\mathrm{SNR(dB)} = 10\log_{10}\left(\frac{\left(\sum_{i=1}^{n} s_i\right)^2}{n\sum_{i=1}^{n} s_i^2-\left(\sum_{i=1}^{n} s_i\right)^2}\right) \tag{3.2}$$

The results are summarized in Table 3.1.

Table 3.1. SNR and FAR Values

Type of Filter	FAR(%) of Q	FAR(%) of T^2	SNR (dB) of Q	SNR(dB) of T^2
Unfiltered signals	0.46	0.79	8.1208	-1.2923
SMF	0.11	0.19	10.2521	13.0327
IMF	0.27	0.52	8.3584	11.2086
Fuzzy logic based filter	0.22	0.48	8.4294	11.3496

Table 3.1 shows the obtained SNR and FAR for the SMF, IMF and the fuzzy logic based filter. The SNR and the FAR of the SMF are better than the ones of the IMF and the fuzzy based filter. These results are due to the filtering process where all the samples are filtered regardless if they are affected by noise or not. This filtering is undesired in fault detection since the sensitivity of the monitoring indices is too much affected. In addition, the filter may return an outlier since its output is the median value within a window of fixed length. Comparing the FAR and the SNR values of the IMF and the fuzzy logic based filter, one can conclude that the fuzzy logic based filter is better than the IMF. The fuzzy logic based filter does not provide satisfactory performances for fault detection because its output is also the median value within a window; hence, it may return an outlier. Therefore, an adjusting parameter is required to control the filtering action where a sample may be just scaled and not totally replaced.

The Fuzzy Logic Filter (FLF) implemented in this work is based on the work of Naso et al [102]. It is developed on the Mamdani Fuzzy Inference System (FIS) with the centroid defuzzification technique [96-100]. Figure 3.2 represents the schematic diagram of the developed FLF. Three inputs are fed to the FIS. These inputs are fuzzified via predefined membership functions. The FIS output is obtained after evaluating the fuzzy rules. The input and output fuzzy sets and the membership functions types are tabulated in Table 3.2.

At the j^{th} iteration a three samples moving window is sliding to scan the data. At this iteration, this window is defined as

$$W_j = [Q_j \quad Q_{j+1} \quad Q_{j+2}] \tag{3.3}$$

Where Q_j is the j element of the unfiltered vector. W_j permits, at each iteration, to compute the FIS inputs which are represented by the following differences

$$d_{1\,j} = Q_j - Q_{(j-1)f} \tag{3.4}$$

$$d_{2\,j} = Q_{j+1} - Q_j \tag{3.5}$$

$$d_{3\,j} = Q_{j+2} - Q_{j+1} \tag{3.6}$$

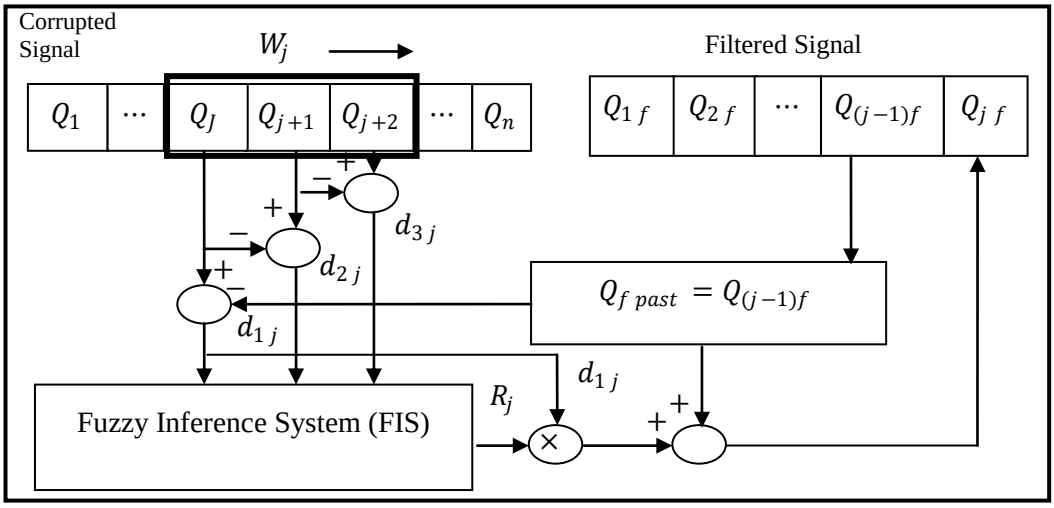

Figure 3.2. Schematic diagram of the FLF

Table 3.2. Fuzzy Sets and Types of Membership Functions for the FLF

Fuzzy input set	Fuzzy output set	Type of Membership Function
LN (Large Negative)	SV (Short Value)	Trapezoidal
ST (Standard)	MV (Medium Value)	Triangular
LP (Large Positive)	LV (Large Value)	Trapezoidal

$Q_{(j-1)f}$ is the filtered sample from the previous iteration.

The FLF algorithm is summarized in the following

1. Define the windowW_j.
2. Compute the FIS inputs.
3. Compute the FIS output $R_j \in [0,1]$

4. Compute the filtered value as

$$Q_{jf} = Q_{(j-1)f} + R(j)\left(Q_j - Q_{(j-1)f}\right) \quad (3.7)$$

The output of the FLF can be either $Q_{(j-1)f}$ when $R_j = 0$ or Q_j when $R_j = 1$ or it is the average of the previous filtered sample and the scaled difference between the actual unfiltered value and the previous filtered one when R_j is between 0 and 1.

3.2.2. Adaptive Thresholds

The adaptive thresholds of the proposed method are generated via the use of a fixed PCA model and a fixed length sliding window. The PCA monitoring indices thresholds depend explicitly on the number of retained PCs and the number of observations in the training data-set. These two parameters are not changing with the proposed method. Referring to the Eq. (2.13), (2.14) and (2.15), the Q threshold depends on the values of the θ_i; therefore, the adaption of the residual subspace thresholds can be achieved if θ_i changes. For that purpose, the variances of the residual subspace, from one time to another and the matrix $\tilde{P}$, are used. The variances are computed for the samples within a specific window length. The projection matrix of the window $wn \in R^{L\times m}$ onto the residual subspace is [96-100]

$$B = wn\tilde{P} = [B_1 \quad B_2 \quad \cdots \quad B_{m-\alpha}] \quad (3.8)$$

wn is first scaled and shifted to zero mean and unity variance.

The θ_i values for $i = 1, 2, 3$ are provided by

$$\theta_i = \sum_{j=1}^{m-\alpha} (var(B_j))^i \quad (3.9)$$

Where $var(.)$ stands for variance.

The adaptive thresholds for the Q statistic is updated using Eq. (2.13) and (2.15) after substituting the values of the θ_i.

The adaptive thresholds of the T^2 monitoring indices is updated empirically by estimating the distribution of the past evaluation of T^2 within a vector of the same length as the length of wn.

3.2.3. Modified Moving Window PCA with Fuzzy Logic Filter Algorithm

The algorithm of the MMWPCA with FLF is performed in two phases: offline and online phases. The offline phase consists of two important tasks in process monitoring which are the process training and the model validation. The first task allows the construction of a descriptive statistical model while the second task permits the model validation. The online phase is used to monitor new testing samples. The two phases are summarized in the following points [96-99]

A. Offline phase

A.1. Process Training

1. Construct the PCA model based on a training data-set. The PCA model is constituted of the mean, standard deviation and the number of PCs.
2. Compute the initial thresholds, Q_{thin} and T^2_{thin}.

A.2. Model Validation

1. Select an appropriate window length of wn that will correspond to minimum FAR in the testing data-set and then set the fault indicator to 0.
2. Apply the constructed PCA model on the testing data-set.
3. Select the fixed thresholds Q_{fixed} and T^2_{fixed}. These thresholds will be employed when a fault is detected. They are set by trial and error in a condition that the process recovery is not affected.
4. Select the fuzzy rules and the parameters of the membership functions for the FLF.

At the end of the offline phase, the PCA model is determined and validated besides to the window length selection and the FLF parameters determination. The identified parameters are then used in the online phase.

B. Online Phase

1. Get the new observation when it is available. Scale and shift it using the mean and standard deviation of the constructed PCA model.
2. Compute its monitoring indices Q and T^2 via the PCA model.
3. Obtain the filtered monitoring indices Q_f and T_f^2 by passing the Q and T^2 through the FLF.
4. Compare the filtered monitoring indices with their associated initial thresholds. If $Q_f < Q_{thin}$ and $T_f^2 < T_{thin}^2$, go to step 6 and 7 otherwise, go to steps 5 and 7.
5. Set the adaptive thresholds as

   $\boldsymbol{Q_{ad}} = Q_{fixed}$ and $T_{ad}^2 = T_{fixed}^2$. Update the initial thresholds as $Q_{thin} = Q_{ad}$ and $T_{thin}^2 = T_{ad}^2$ and switch the fault indicator to 1.

6. Include the sample in the wn after excluding the first observation. Recalculate the new thresholds and set $\boldsymbol{Q_{thin}} = Q_{ad}$ and $T_{thin}^2 = T_{ad}^2$. Set the fault indicator to 0.
7. Repeat from 1.

Figure 3.3 summarizes the algorithm where all the necessary steps are presented.

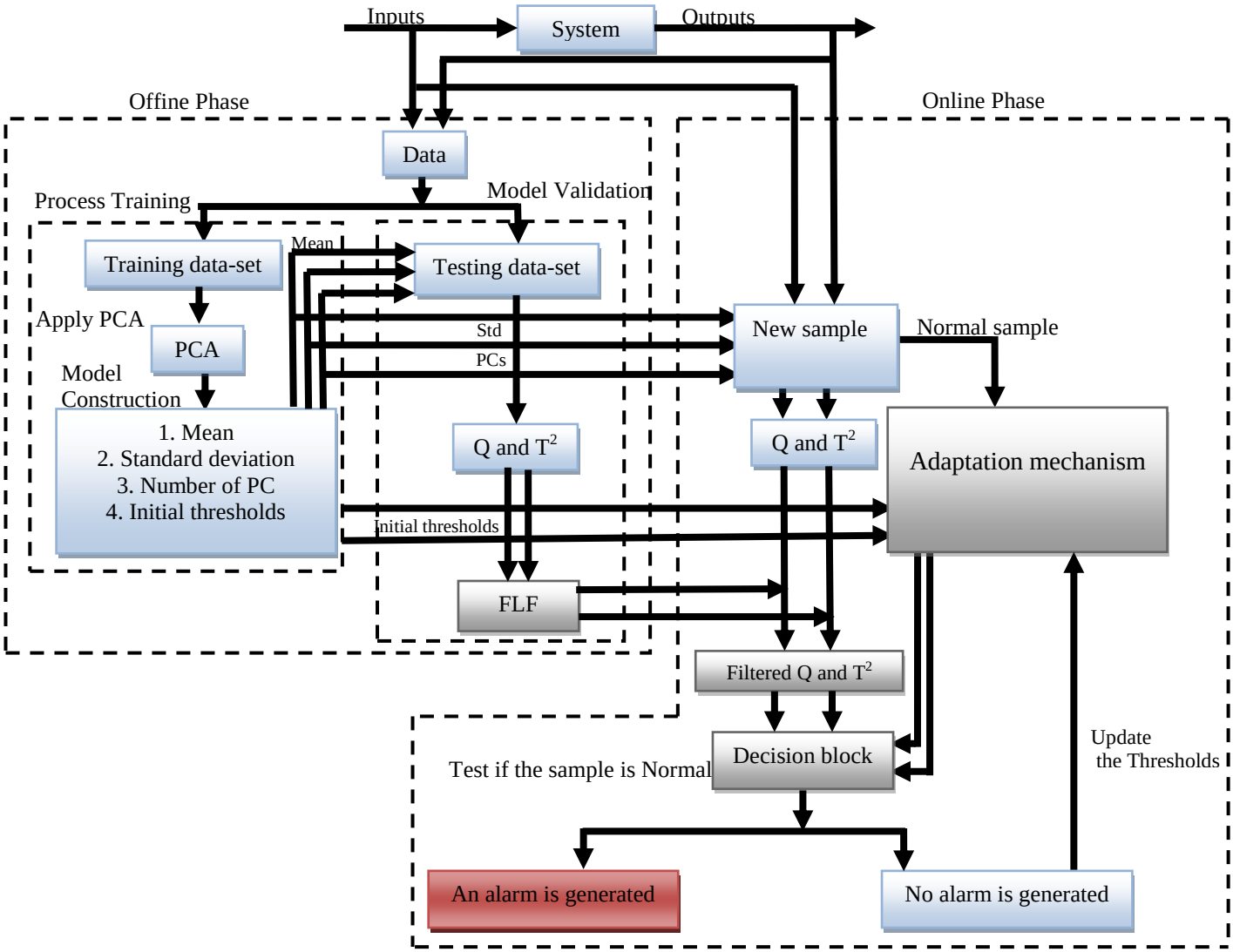

Figure 3.3. Application procedure of the MMWPCA with FLF

The MMWPCA with FLF based fault detection technique does not take into consideration the relationships between the current sample and the past observations. To include the dynamic behavior of the data in the statistical model, the MMWPCA with FLF method has been extended to Modified Moving Window Dynamic PCA (MMW-DPCA) with Fuzzy Logic Filter (FLF). The same steps of the MMWPCA with FLF algorithm are performed in the MMW-DPCA with FLF algorithm except that the lags are added to the data.

3.3. Modified Moving Window Dynamic PCA with Fuzzy Logic Filter

The filter's design procedure for this method is the same as the FLF described above. The adaptive thresholds generation steps are the same as the MMWPCA with FLF monitoring scheme. The only difference is that a number of lags, *l*, is added to the moving window *wn*. To distinguish between the two moving windows, let wn_{aug} denote the augmented moving window. After the number of needed lags, *l*, is determined using any algorithm given in [31]; The following MMW-DPCA with FLF algorithm can be applied for the process monitoring [100]

A. Offline Phase

1. Add *l* to the training data matrix then apply PCA to determine the statistical model.
2. Initiate the control limits Q_{thin} and T^2_{thin} for this data-set.
3. Initiate the fault indicator to 0 and select the appropriate length for the wn_{aug}
4. Select the fixed thresholds, Q_{fixed} and T^2_{fixed}. These thresholds will be employed when a fault is detected. They are set by trial and error in a condition that the process recovery is not affected.
5. Select the fuzzy rules and the parameters of the membership functions for the FLF.

B. **Online Phase**

1. Get the new testing sample when it is available. Add to it *l* lags. Scale and shift the observation using the mean and standard deviation of the constructed DPCA model.
2. Evaluate its corresponding Q and T^2.

3. Obtain the filtered monitoring indices Q_f and T_f^2 by passing the Q and T^2 through the FLF.
4. Compare the filtered monitoring indices with their associated initial thresholds. If $Q_f < Q_{thin}$ and $T_f^2 < T_{thin}^2$, go to step 6 and 7 otherwise, go to steps 5 and 7.
5. Set the adaptive thresholds as

   $Q_{\boldsymbol{ad}} = Q_{fixed}$ and $T_{ad}^2 = T_{fixed}^2$. Update the initial thresholds as $Q_{thin} = Q_{ad}$ and $T_{thin}^2 = T_{ad}^2$. Switch the fault indicator to 1.

6. Include the sample in the wn_{aug} after excluding the first observation. Recalculate the new thresholds and set $Q_{\boldsymbol{thin}} = Q_{ad}$, $T_{thin}^2 = T_{ad}^2$ and the fault indicator to 0.
7. Repeat from 1.

The offline phase of the MMW-DPCA with FLF permits to construct the DPCA model. In addition, it allows the selection of the moving window length and the FLF parameters. The online phase is used to monitor new testing samples. The MMW-DPCA algorithm is summarized by the following flowchart.

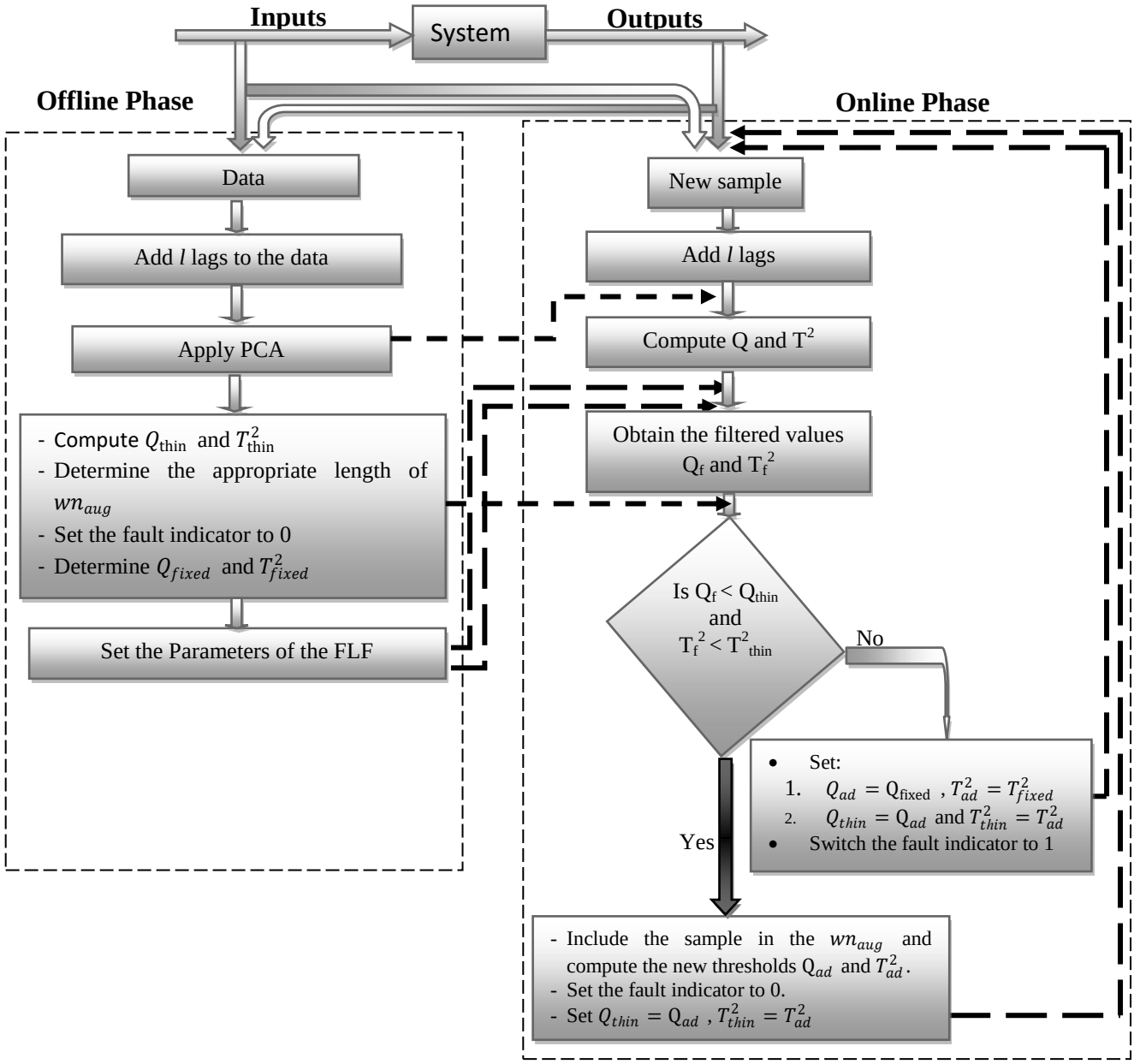

Figure 3.4. Flowchart of the MMW-DPCA with FLF [100]

In this chapter, the three proposed methods have been presented. The CFAR method focuses on the number of false alarms to detect faults whereas the MMWPCA and MMW-DPCA with FLF combine the advantages of PCA or DPCA and the MWPCA to monitor processes via fixed statistical model and adaptive thresholds. The adaptive thresholds will improve the monitoring indices sensitivity while the use of the FLF will enhance the fault detection accuracy by reducing the effect of false alarm in the process monitoring. The applications of these methods are provided in the next chapter.

Chapter Four

Applications: Results and Discussions

The applications of the proposed methods are presented in this chapter. The CFAR technique has been applied to the Cement Rotary Kiln (CRK) of Ain El Kebira. The MMWPCA with FLF has been applied to the Tennessee Eastman Process (TEP), CRK and a Grid-Connected Photovoltaic System (GCPVS). The application of the MMW-DPCA with FLF has been carried out on the TEP and CRK. The organization of this chapter is as follows. Section 4.1 is devoted to the descriptions of different processes to which the proposed methods are applied. Section 4.2 is about the results and discussions of the CFAR application on CRK, the application of the MMWPCA and MMW-DPCA with FLF on the old model of the TEP and the application of the MMWPCA with FLF on the revised model of the TEP; furthermore, the application results of the MMWPCA with FLF on the GCPS are presented and discussed also in this section.

4. Applications: Results and Discussions

4.1. Process Description

4.1.1. Cement Rotary Kiln

Cement plant of Ain El Kebira is the first production line in Algeria. The experimental application of the developed monitoring schemes has been performed on its rotary kiln. This rotary kiln is about 80 m length and 5.4 m in diameter, inclined by 3 degrees. Rotary kilns are used to heat materials to a temperature at which the chemical reactions occur allowing the production of cement substance. Figure 4.1 shows the cement plant divided into two parts (a) and (b) following material flow direction, from the top of the pre-heater tower downwards to the cooler [100]. Two 560 kW asynchronous motors rotate the kiln at a maximum speed of 2.14 rpm. A series of four cyclones, mounted on four floors of two parallel towers, are used to dry and hydrate the raw materials via the hot counter stream gas and a secondary fuel burner mounted in the bottom of the towers. The kiln’s rotation causes the gradual downstream

motion of the entered pre-heated mixture to the kiln's lower end. During this motion, the material is further heated using the main burner and hot secondary gas coming back from the cooler. At high temperatures (more than 1450 C°), a liquid phase appears and complex chemical reactions are sped up before entering vitrification phase where materials become again solid but in a new structural form called clinker. The clinker is then milled with some additives to produce cement. As a last step in the cement production, the kiln's output is cooled down to less than 100 C° via the cooler of many fans, static and mobile gates. [91, 95, 97, 100, 103-104].

Figure 4.1-b. Cooler system with its heat exchanger and filter to the left and kiln end appears to right.

Figure 4.1-a. Pre-heater tower at the right along with rotary kiln laying in horizontal to the left.

Figure 4.1. Ain El Kebira cement plant.

Table 4.1. Measured variables of the cement rotary kiln

Variable	Sensor's Tag	Description	Unit
x_1	229_32/SE	Process filter exhauster fan speed for tower I	r.p.m
x_2	239_32/SE	Process filter exhauster fan speed for tower II	r.p.m
x_3	313_03/FE	Raw materials flow rate feeding the kiln's tower I	Tones/h
x_4	313_04/FE	Raw materials flow rate feeding the kiln's tower II	Tones/h
x_5	331_01/PE	Cyclone I outlet gas's negative pressure for tower I	mbar
x_6	331_01/TE	Cyclone I outlet gas's temperature for tower I	C°
x_7	331_02/PE	Cyclone II outlet gas's negative pressure for tower I	mbar
x_8	331_02/TE	Temperature of gases in outlet of cyclone II, tower I	C°
x_9	331_03/PE	Depression of gases in outlet of cyclone III, tower I	mbar
x_{10}	331_03/TE	Temperature of gases in outlet of cyclone III, tower I	C°
x_{11}	331_04_PE	Depression of gases in outlet of cyclone IV, tower I	mbar
x_{12}	331_04/TE	Temperature of gases in outlet of cyclone IV, tower I	C°
x_{13}	331_05/JE(P)	Exhauster fan motor's power for tower I	KW
x_{14}	331_05_PE	Depression of gases in inlet of cyclone IV, tower I	mbar
x_{15}	331_05/SE	Speed of the exhauster fan of tower I	r.p.m
x_{16}	331_05/TE	Temperature of the materials entering the kiln, tower I	C°
x_{17}	331_06/PE	Depression of gases in outlet of smoke box, tower I	mbar
x_{18}	331_07/TE	Temperature of gases in outlet of smoke box, tower I	C°

x_{19}	335_05/JE(P)	Power of the motor of the exhauster fan, tower II	KW
x_{20}	335_05/SE	Speed of the exhauster fan of tower II	r.p.m
x_{21}	341_01/PE	Depression of gases in outlet of cyclone I, tower II	mbar
x_{22}	341_01/TE	Temperature of gases in outlet of cyclone I, tower II	C°
x_{23}	341_02/PE	Depression of gases in outlet of cyclone II, tower II	mbar
x_{24}	341_02/TE	Temperature of gases in outlet of cyclone II, tower II	C°
x_{25}	341_03/PE	Depression of gases in outlet of cyclone III, tower II	mbar
x_{26}	341_03/TE	Temperature of gases in outlet of cyclone III, tower II	C°
x_{27}	341_04/PE	Depression of gases in outlet of cyclone IV, tower II	mbar
x_{28}	341_04/TE	Temperature of gases in outlet of cyclone IV, tower II	C°
x_{29}	341_05/PE	Depression in inlet of cyclone IV, tower II	mbar
x_{30}	341_05/TE	Temperature of materials in the in inlet of cyclone IV, tower II	C°
x_{31}	341_06/PE	Smoke box outlet gas's negative pressure for tower II	mbar
x_{32}	341_07/TE	Temperature of gases in outlet of smoke box, tower II	C°
x_{33}	351_01/JE	Kiln's spinning motors power (sum of two)	KW
x_{34}	351_03/SE	Kiln's rotation speed	r.p.m
x_{35}	355_08/TE	Temperature of the excess air from the cooler	C°
x_{36}	355_10/PE	Static grate cooling fan I air pressure	mbar
x_{37}	355_10/SE	Static grate cooling fan's I speed	r.p.m
x_{38}	355_11/TE	Secondary air temperature	C°
x_{39}	355_12/PE	Pressure of the air under the static grate (repression fan II)	mbar
x_{40}	355_14/PE	Pressure of the air under the static grate (repression fan III)	mbar
x_{41}	355_14/SE	Speed of the cooling fan III	r.p.m
x_{42}	355_16/PE	Pressure of the air under chamber I of the dynamic grate(repression fan IV)	mbar
x_{43}	355_16/SE	Speed of fan IV	r.p.m
x_{44}	355_18/PE	Pressure of the air under chamber II of the static grate	mbar
x_{45}	355_18/SE	Speed of the cooling fan V	r.p.m
x_{46}	355_20/PE	Pressure of the air under chamber III of the dynamic grate(repression fan VI)	mbar
x_{47}	355_20/SE	Speed of the cooling fan VI	r.p.m
x_{48}	355_62/ST	Speed of the dynamic grate	Strockes.p.m
x_{49}	ACM01_01/SIC _LMN	Kiln's head-hood pressure controller output controlling the cooler filter exhaust fans	r.p.m
x_{50}	AGN_04/FE	Flow of fuel (natural gas) to the main burner	m^3/h
x_{51}	HO1_PY/FE	Flow of fuel (natural gas) to the secondary burner in the pre-calcination level	m^3/h

4.1.2. Tennessee Eastman Process (Old Model)

Tennessee Eastman Process (TEP) was created by Eastman company to test and simulate the variety of the developed methods in the field of process control and process monitoring [65]. The simulator was developed by Downs and Vogel [105-107]. The system is composed of five major units, a reactor, a product condenser, a vapor liquid separator, a recycle compressor and a product stripper [108-114]. Figure 4.2 shows the TEP diagram. The measured variables and the manipulated variables of the TEP are tabulated in Table 4.2 and Table 4.3. The simulator permits to simulate 21 faults. These faults are listed in Table 4.4.

Sixteen of the TEP faults are known while the remaining disturbances are unknown. The first 7 faults correspond to the step change in the process variables. The 8th up to the 12th fault are related to an increase variability of some process variables. Fault 13 is a slow drift in the reactor kinetics and faults 14, 15 and 21 are associated with the sticking valves [96, 99-100].

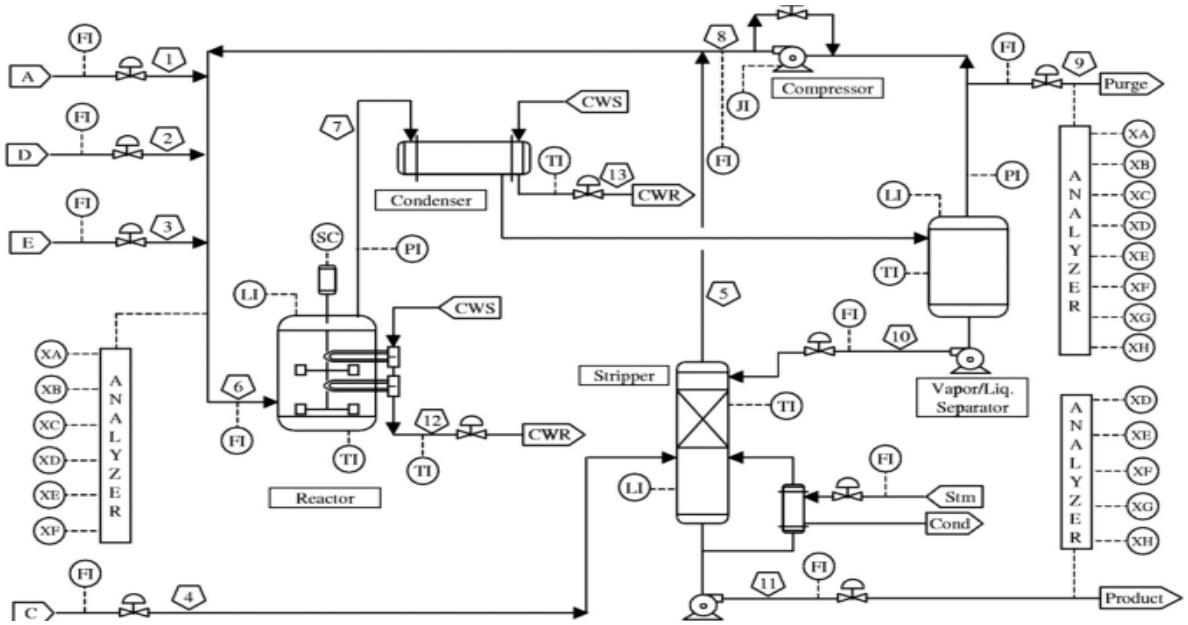

Figure 4.2. Tennessee Eastman process diagram

Table 4.2. Manipulated Variables

Variable	Description
XMV(1)	D Feed Flow (Stream 2)
XMV(2)	E Feed Flow (Stream 3)
XMV(3)	A Feed Flow (Stream 1)
XMV(4)	Total Feed Flow (Stream 4)
XMV(5)	Compressor Recycle Valve
XMV(6)	Purge Valve (Stream 9)
XMV(7)	Separator Pot Liquid Flow (Stream 10)
XMV(8)	Stripper Liquid Product Flow (Stream 11)
XMV(9)	Stripper Steam Valve
XMV(10)	Reactor Cooling Water Flow
XMV(11)	Condenser Cooling Water Flow
XMV(12)	Agitator Speed

Table 4.3. Measured Variables

Variable	*Description*	*Variable*	*Description*
XMEAS(1)	A Feed (Stream 1)	XMEAS(22)	Separator Cooling Water Outlet Temp
XMEAS(2)	D Feed (Stream 2)	XMEAS(23)	Composition of A in Reactor Feed
XMEAS(3)	E Feed (Stream 3)	XMEAS(24)	Composition of B in Reactor Feed
XMEAS(4)	Total Feed (Stream 4)	XMEAS(25)	Composition of C in Reactor Feed
XMEAS(5)	Recycle Flow (Stream 8)	XMEAS(26)	Composition of D in Reactor Feed
XMEAS(6)	Reactor Feed Rate (Stream 6)	XMEAS(27)	Composition of E in Reactor Feed
XMEAS(7)	Reactor Pressure	XMEAS(28)	Composition of F in Reactor Feed
XMEAS(8)	Reactor Level	XMEAS(29)	Composition of A in Purge Gas Flow
XMEAS(9)	Reactor Temperature	XMEAS(30)	Composition of B in Purge Gas Flow
XMEAS(10)	Purge Rate (Stream 9)	XMEAS(31)	Composition of C in Purge Gas Flow
XMEAS(11)	Product Sep Temp	XMEAS(32)	Composition of D in Purge Gas Flow

XMEAS(12)	Product Sep Level	XMEAS(33)	Composition of E in Purge Gas Flow
XMEAS(13)	Prod Sep Pressure	XMEAS(34)	Composition of F in Purge Gas Flow
XMEAS(14)	Prod Sep Underflow (Stream 10)	XMEAS(35)	Composition of G in Purge Gas Flow
XMEAS(15)	Stripper Level	XMEAS(36)	Composition of H in Purge Gas Flow
XMEAS(16)	Stripper Pressure	XMEAS(37)	Composition of D in Product Flow
XMEAS(17)	Stripper Underflow (Stream 11)	XMEAS(38)	Composition of E in Product Flow
XMEAS(18)	Stripper Temperature	XMEAS(39)	Composition of F in Product Flow
XMEAS(19)	Stripper Steam Flow	XMEAS(40)	Composition of G in Product Flow
XMEAS(20)	Compressor Work	XMEAS(41)	Composition of H in Product Flow
XMEAS(21)	Reactor Cooling Water Outlet Temp		

Table 4.4. Process Faults of TEP

Fault NO	Description	Type	Fault NO	Description	Type
1	A/C Feed ration, B Composition constant(Stream 4)	Step	**13**	Reaction kinetics	Slow drift
2	B Composition, A/C ration constant (Stream4)	Step	**14**	Reactor cooling water valve	Sticking
3	D Feed temperature (Stream 2)	Step	**15**	Condenser cooling water valve	Sticking
4	Reactor cooling water inlet temperature	Step	**16**	Unknown	Unknown
5	Condenser cooling water inlet temperature	Step	**17**	Unknown	Unknown
6	Feed loss (Stream 1)	Step	**18**	Unknown	Unknown
7	C Header pressure loss- Reduced availability (Stream 4)	Step	**19**	Unknown	Unknown
8	A, B, C feed composition (Stream 4)	Random Variation	**20**	Unknown	Unknown
9	D Feed temperature (Stream 2)	Random Variation	**21**	Valve position constant (Stream 4)	Constant position
10	C Feed temperature (Stream 4)	Random Variation			
11	Reactor cooling water inlet temperature	Random Variation			
12	Condenser cooling water inlet temperature	Random Variation			

4.1.3. Tennessee Eastman Process (Revised Model)

The TEP described above has been revised by Bathelt et al [115] where they added some measured variables which are listed in Table 4.5; thus, the revised model provides 85 measured variables in which two of them are constant. The new model permits to simulate 28 faults. Table 4.6 represents the revised TEP faults [99].

Table 4.5. Added variables

Variable	Description
XMEAS(42)	Temperature A Feed (Stream 1)
XMEAS(43)	Temperature D Feed (Stream 2)
XMEAS(44)	Temperature E Feed (Stream 3)
XMEAS(45)	Temperature A and C Feed (Stream 4)
XMEAS(46)	Reactor Cooling Water Inlet Temperature
XMEAS(47)	Reactor Cooling Water Flow
XMEAS(48)	Condenser Cooling Water Inlet Temperature
XMEAS(49)	Condenser Cooling Water Flow
XMEAS(50- 55)	Composition of A Feed (Stream1); Components A through F
XMEAS(56- 61)	Composition of D Feed (Stream2); Components A through F
XMEAS(62- 67)	Composition of E Feed (Stream3); Components A through F
XMEAS(68- 73)	Composition of A and C Feed (Stream4); Components A through F

Table 4.6. Process Faults

Fault NO	Description	Type	Fault NO	Description	Type
1	A/C Feed ration, B Composition constant(Stream 4)	Step	**15**	Condenser cooling water valve	Sticking
2	B Composition, A/C ration constant (Stream4)	Step	**16**	Unknown	Unknown
3	D Feed temperature (Stream 2)	Step	**17**	Unknown	Unknown
4	Reactor cooling water inlet temperature	Step	**18**	Unknown	Unknown
5	Condenser cooling water inlet temperature	Step	**19**	Unknown	Unknown
6	Feed loss (Stream 1)	Step	**20**	Unknown	Unknown
7	C Header pressure loss- Reduced availability (Stream 4)	Step	**21**	A feed temperature (stream 1)	Random Variation
8	A, B, C feed composition (Stream 4)	Random Variation	**22**	E feed temperature (stream 3	Random Variation
9	D Feed temperature (Stream 2)	Random Variation	**23**	A feed pressure (stream 1)	Random Variation
10	C Feed temperature (Stream 4)	Random Variation	**24**	D feed pressure (stream 2)	Random Variation
11	Reactor cooling water inlet temperature	Random Variation	**25**	E feed pressure (stream 3)	Random Variation
12	Condenser cooling water inlet temperature	Random Variation	**26**	A and C feed pressure (stream 4)	Random Variation
13	Reaction kinetics	Slow drift	27	pressure fluctuation in the cooling water re-circulating unit of the reactor	Random Variation
14	Reactor cooling water valve	Sticking	28	pressure fluctuation in the cooling waterre-circulating unit of the condenser	Random Variation

4.1.4. Grid-Connected Photovoltaic System.

The Grid-Connected Photovoltaic System (GCPVS), of the Power Electronic and Renewable Energy Research Laboratory (PEARL) of Malaya University, supplies the power to the laboratory building [116]. The detailed information about this system is tabulated in Table 4.7 [117]. This GCPVS is composed of 16 modules of polycrystalline silicon (POLY), 25 modules of monocrystalline (MONO) and 20 modules of the thin film. These modules are connected to the three inverters INV 01, INV 02 and INV 03 respectively. Figure 4.3 shows the diagram of the GCPVS. The list of measured variables consists mainly of the solar radiation, wind speed, panels' and ambient temperatures, voltages and currents at different stages.

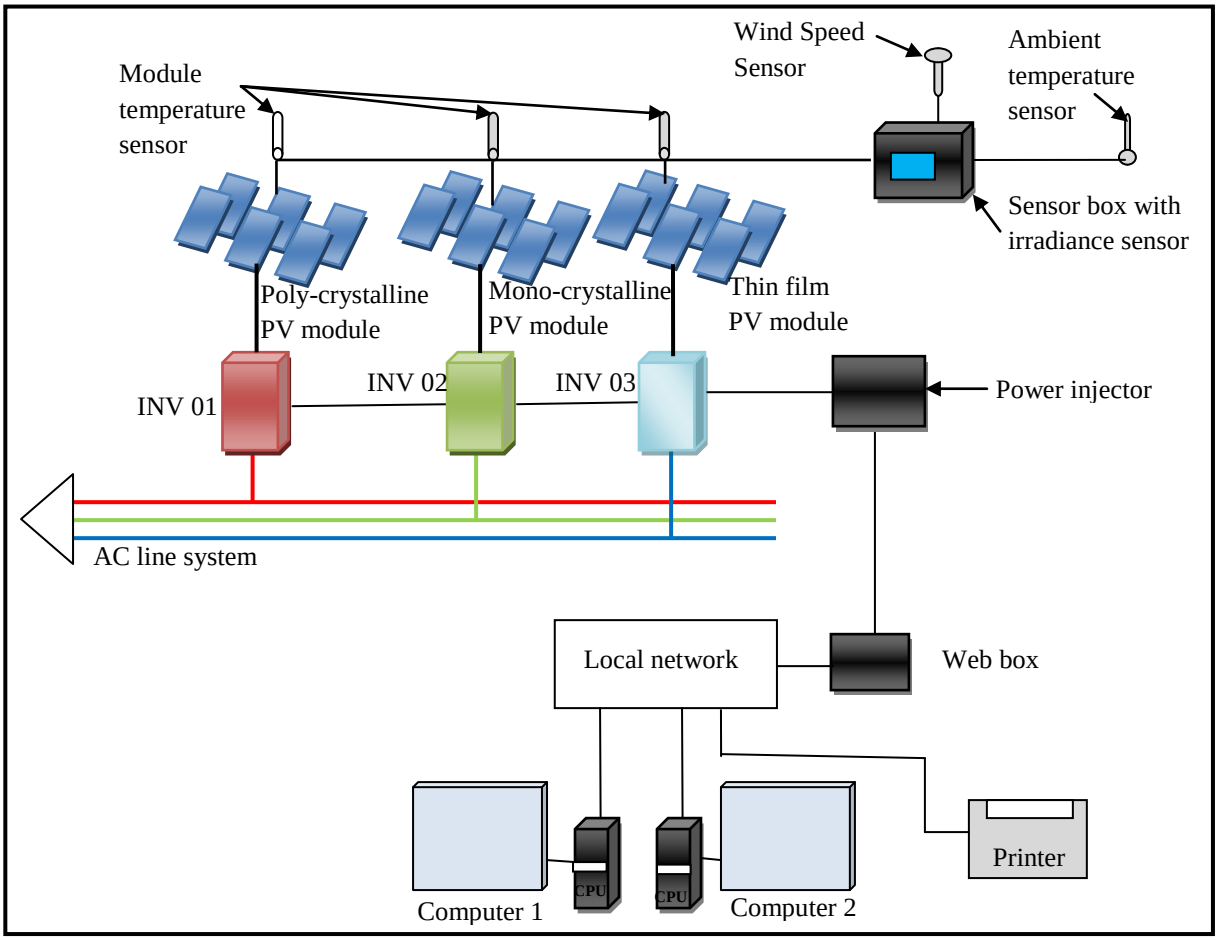

Figure 4.3. Schematic diagram of grid-connected PV system

Table 4.7. Process Description

Specifications	Polycrystalline	Monocrystalline	Thin film
Number of modules	16	25	20
DC power per module (Wp)	125	75	135
Voltage at max. power (V)	17.3	47.0	17.0
Current at max. power (A)	7.9	2.9	4.4
DC/ AC inverter capacity (W)	1600	1600	2500
Inverter max. DC voltage (V)	600	600	700
Inverter max. AC voltage (V)	220-240	220-240	220-240

4.2. Results and Discussions

4.2.1. Application of CFAR on the Cement Rotary Kiln

The CFAR based fault detection is applied to the cement rotary kiln presented above. This technique has been used with the PCA method. Under healthy operation conditions of the CRK, 15344 observations were collected for 51 measured variables. These variables are

provided in the Table 4.1. The data have been recorded with one sample every one second. These data have been processed to remove outliers and corrupted observations using a statistical filter where all the observations with values greater than $\mu \pm 3\sigma$ have been removed, where μ is the mean and σ the standard deviation of each measured variable. After data processing, a training data- set of 14730 samples is employed to construct the PCA model. The fixed thresholds of the PCA monitoring indices are calculated with 99% Confidence Level (CL). By means of the CPV, which is set at 90%, 28 principal components have been retained [95]. The monitoring indices along with their corresponding fixed thresholds are depicted in Figure 4.4.

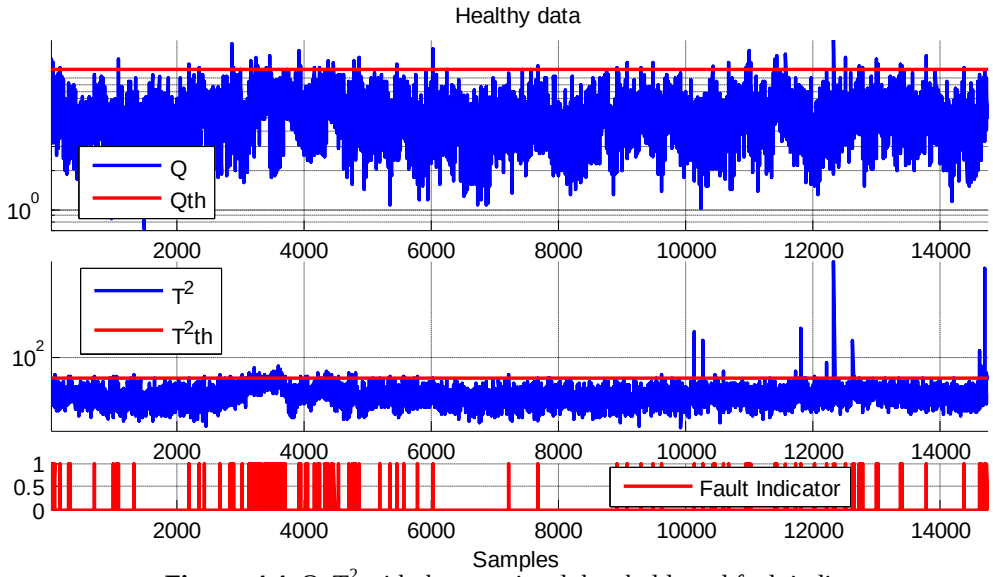

Figure 4.4. Q, T^2 with the associated thresholds and fault indicator

The problem of false alarms is clearly seen from this figure. 184 false alarms are recoded. From the fault indicator, the detection accuracy of any possible fault is much affected by the presence of these false alarms. The monitoring indices of some observations violate the control limit indicating that abnormal behavior has been occurred, however, the data have collected during the healthy mode of the CRK. The CFAR method has been applied to the same data-set. But before the application, the length of the moving window must be first determined. This length is selected based on the minimum FAR in the training data-set. The

window length selected for this application is 1031 [95]. The CFAR monitoring indices with their corresponding thresholds are presented in Figure 4.5.

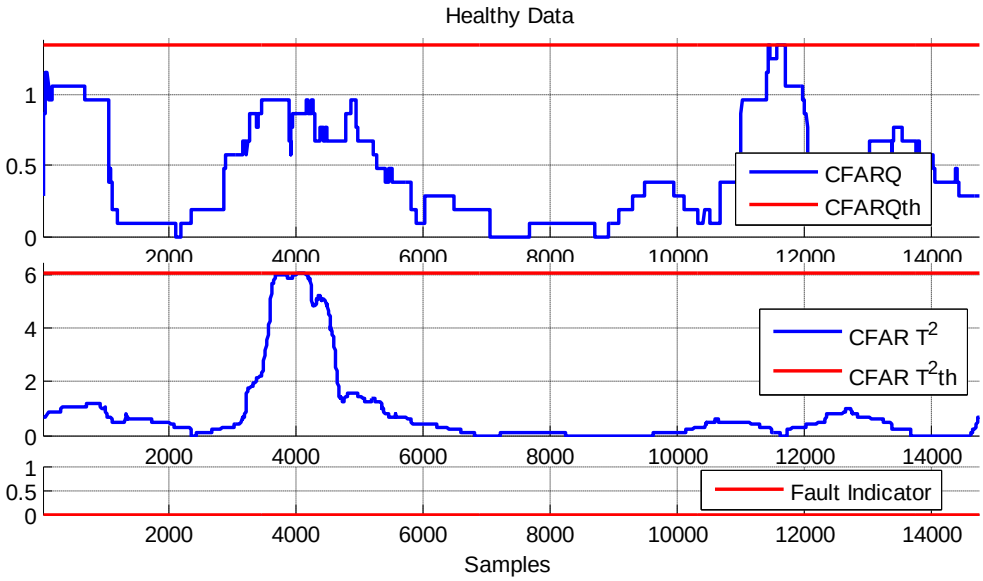

Figure 4.5. CFARQ, CFART^2 with the associated thresholds and fault indicator

It can be shown from Figure 4.5 that no false alarm has been signaled with the CFAR method, hence, this method resolved the problem of the false alarms encountered by the PCA based monitoring scheme. The CFAR detection ability is tested using abrupt fault, intermittent fault and ramp fault. These faults are injected in the data. The descriptions of the faults, the resulted FAR and the detection delay are in the Table 4.8.

Table 4.8. Fault Description, the FAR and the Detection Delay

Fault Type	Occurrence Time (sec)	Amplitude %	Sensor's Number	Detection Delay (sec)	FAR %
Abrupt	9000	3	8	12	0
Intermittent	9000	3	28	12	0
Ramp	9000		4	234	0

Table 4.8 shows that the resulted FAR for the sensors faults are 0%. The CFAR technique, as it is illustrated by this table, introduces a delay of 12 sec for the abrupt and the intermittent faults while 234 sec for the ramp fault. The relatively high detection delay of the ramp fault is due to its slope which is taken very small to simulate the worst case.

The detection of the real fault by the CFAR is in the following figure

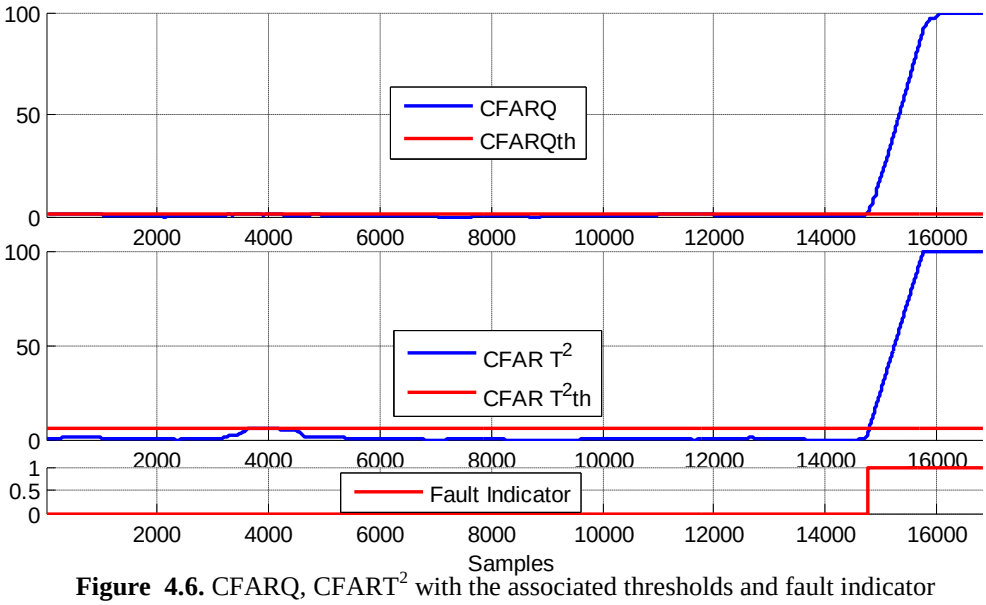

Figure 4.6. CFARQ, CFART^2 with the associated thresholds and fault indicator

Figure 4.6 confirms the occurrence of a fault since some samples are above the thresholds. It is also seen that this fault has been detected with no false alarm.

4.2.2. Application of MMWPCA and MMW-DPCA with FLF to the Old TEP Model

The MMWPCA and MMW-DPCA with FLF have been applied to the old model of the TEP. The proposed monitoring schemes have been applied to the same benchmark data-sets used by Russell et al [58]. 52 measured variables were employed. The number of observations in the training data-set is 500 while a total of 960 samples are in the testing and the faulty data-sets. All the measurements were sampled every 3 minutes. The faults in the faulty data-sets were introduced after 8 simulation hours.

The PCA and the DPCA models have been constructed and validated based on the training and testing (Fault 0) data-sets. The dynamic structure of the MMW-DPCA with FLF is the same as the one provided by Russell et al [58] where 3 lags are used. The PCA model of the MMWPCA with FLF is determined by 11 PCs which captures 54% of the total variance. On the other side, the DPCA model of the MMW-DPCA with FLF is described by 29 PCs explaining 61.39% of the total variance. The initial thresholds and the adaptive thresholds of

the proposed methods are calculated at 99% CL. The fixed thresholds are determined by trial and error. The sliding windows lengths and the filters parameters are selected based on the minimum FAR recorded for the testing data-set. Two approaches of MMWPCA with FLF have been implemented, the hold-five and the hold-one. The obtained FAR, MDR and the detection delay are tabulated in Tables 4.9, 4.10, and 4.11. These results are compared against the results of Russell et al. [58], Rato et al [33], Yu and Khan [56] and Wang et al [118]. Table 4.12 represents the detailed comparison (method against method) [96-100].

Table 4.9. FAR for the Training and the Testing Data-Sets

Methods	Russell et al [58] PCA		Russell et al [58] DPCA		MMW-DPCA		Hold-five MMWPCA		Hold-one MMWPCA	
Statistics	**Q**	**T^2**	**Q**	**T^2**	**Q**	**T^2**	**Q**	**T^2**	**Q**	**T^2**
Training Data-Set	0.4	0.2	0.4	0.2	**0**	**0**	**0**	**0**	**0**	**0**
Testing Data-Set	1.6	1.4	28.1	0.6	**0**	**0**	**0**	**0**	**0**	**0**

Table 4.10. Missed Detection Rate for the 21 Faults

Methods	Russell et al [58] PCA		Russell et al [58] DPCA		Rato et al[33] MWPCA		Rato et al[33] RPCA		Yu and Khan [56] NGSSM		Yu and Khan [56] NDPCA		Wang et al [118] LPPLS		MMW-DPCA		Hold-five MMWPCA		Hold-one MMWPCA	
Statistics	**Q**	**T^2**	**Q**	**T^2**	**Q**	**T^2**	**Q**	**T^2**	**Q**	**T^2**	**Q**	**T^2**	**Q**	**T^2**	**Q**	**T^2**	**Q**	**T^2**	**Q**	**T^2**
Fault No																				
1	0.3	0.8	0.5	0.6	0.4	0.6	0.9	0.9	0.75	0.38	0.5	0.5	0.62	1	0.62	0.62	1	1.5	0.62	0.87
2	1.4	2	1.5	1.9	3.1	1.9	3.2	1.7	1.75	1.62	1.5	1.88	2	2	1.50	**1.62**	2.37	2.37	1.62	1.87
3	99.1	99.8	99	99.1	99.6	99.4	99.8	99.9	97.7	97.1	96.7	97.6	99.7	99.6	99.2	100	100	100	100	100
4	3.8	95.6	0	93.9	99.4	99.4	8.90	85.6	92.7	89.5	87.7	86.2	13.7	99.7	0.25	**54.4**	0.62	**35.7**	0.12	**73.3**
5	74.6	77.5	74.8	75.8	78.5	76.7	90.1	77.9	70	58.3	61.5	64.2	0	1.87	51.4	64	71	72.7	70.8	72.7
6	0	1.1	0	1.3	0.1	0.5	0.10	0.7	0	0	0	0	0	1	0.12	0.5	3	3	0.12	0.87
7	0	8.5	0	15.9	6.0	0.1	30	0.1	51.6	39.1	46.4	50.3	0	63.6	0.12	6.38	0.62	0.75	0.12	0.12
8	2.4	3.4	2.5	2.8	3.2	2.9	15.6	2.9	1.75	1.38	1.75	2.25	5.87	8	2.62	2.62	3.15	3.25	2.62	2.87
9	98.1	99.4	99.4	99.5	99.9	99.9	100	99.8	98	99.8	97.6	98.7	99.5	99.1	**91.7**	**92.1**	**85.6**	**89.1**	98.3	98.8
10	65.9	66.6	66.5	58	98.9	98.4	99.6	99.6	33.2	17.3	41.6	43.2	83.1	67.5	**23.7**	31.2	52.1	62.2	33.6	48.3
11	35.6	79.4	19.3	80.1	98.4	98.1	93.5	92.3	67.7	70.5	70.3	76.2	41.7	97.1	**4.13**	**35.6**	**5.25**	**34.6**	**4**	**38.6**
12	2.5	2.9	2.4	1	2.7	1.7	13.5	2.0	2.12	4	2.13	2.63	3.75	7.75	**0.37**	**0.37**	**0.87**	**1**	**0.37**	**0.37**
13	4.5	6	4.9	4.9	0.2	2.4	6	5.7	5.37	3.62	5.26	5.51	6.37	5.87	4.88	4.88	5.25	6.25	4.75	6.13
14	0	15.8	0	6.1	0.1	0.1	12.6	1.9	0.12	0.25	8.01	9.26	0	97.6	0.25	0.37	0.75	1.37	0.25	0.25
15	97.3	98.8	97.6	96.4	99.8	99.0	99.8	100	83.7	67.2	71.8	70.2	99.7	99.5	92.9	93.9	97.6	99.5	81.8	87.9
16	75.5	83.4	70.8	78.3	99.6	99.9	99.5	100					73.1	60.6	**41.9**	**54.6**	**42**	**49.1**	**47.4**	65.9
17	10.8	25.9	5.3	24	78.2	80.3	10.9	24.6					14.3	58.5	**2.87**	**7.50**	**3.62**	**9.37**	**3.25**	**3.62**
18	10.1	11.3	10	11.1	11.2	11.0	10.5	10.9					10.7	12.6	10.3	11.2	11.3	12	10.7	11.2
19	87.3	99.6	73.5	99.3	99.5	99.3	100	99.6					95.2	99.3	**30.6**	**84.7**	**2.87**	**76.2**	98.4	99.8
20	55	70.1	49	64.4	94	92.6	90.6	89.8					64.8	64.3	**19.6**	**28.9**	**14.6**	**28**	**11.6**	**35.1**
21	57.0	73.6	55.8	64.4	98.9	98.5	100	100					60.7	59.8	**36.2**	**44.5**	**37.7**	**52.2**	**35.7**	64.4
MMDR	37.2	48.6	34.8	46.6	55.7	55.3	51.6	52.1	40.4	36.6	39.5	40.5	36.8	52.6	**24.5**	**34.2**	**25.7**	**35.2**	**28.8**	38.7

Blank cell means that the MDR is not reported.

Table 4.11. Detection Time Delay (Samples)

Methods	Russell et al [58] PCA		Russell et al [58] DPCA		MMW-DPCA		Hold-five MMWPCA		Hold-one MMWPCA	
Statistics / Fault No	Q	T^2	Q	T^2	Q	T^2	Q	T^2	Q	T^2
1	3	7	5	6	5	**5**	9	14	5	7
2	12	17	13	16	**12**	**13**	19	25	13	**15**
3					**514**					
4	3		1	151	2	**3**	6	**14**	**1**	**1**
5	1	16	2	2	2	3	7	14	2	3
6	1	10	1	11	**1**	**4**	6	30	**1**	**1**
7	1	1	1	1	**1**	2	6	11	**1**	**1**
8	20	2 3	21	23	21	**21**	25	31	21	**23**
9					**660**	**660**	**333**	**340**	**363**	**662**
10	49	96	50	101	**26**	**26**	60	430	51	**53**
11	11	304	7	195	**7**	**9**	12	**21**	11	**12**
12	8	22	8	3	**3**	**3**	**8**	13	**3**	**3**
13	37	49	40	45	39	**39**	43	52	38	49
14	1	4	1	6	2	**3**	7	12	2	**2**
15	740				**238**	**242**	**243**	**248**	**580**	**581**
16	197	312	196	199	**22**	**26**	203	208	199	**199**
17	25	29	24	28	**23**	**28**	30	35	26	**28**
18	84	93	84	93	**83**	**90**	92	97	86	**90**
19			82		**16**	**16**	**16**	**62**	**12**	**13**
20	87	87	84	89	**81**	**82**	90	95	**83**	**83**
21	285	563	286	522	**251**	**257**	**261**	**276**	**244**	**456**

Blank cell means that the detection delay is not reported or a fault is not detected.

Table 4.12. Method Against Method Comparison

Methods		Russell et al [58] PCA	Russell et al [58] DPCA	Rato et al [33] MWPCA	Rato et al [33] RPCA	Wang et al [56] LPPLS	Yu and Khan*[118] NGSSM	Yu and Khan*[118] NDPCA
Statistics								
MMW-DPCA	**Q**	**57.14**	**61.90**	**80.95**	**95.24**	**80.95**	**66.67**	**60**
	T^2	**95.24**	**85.71**	**76.19**	**85.71**	**90.48**	40	**66.67**
Hold-five MMWPCA	**Q**	**52.38**	**52.38**	**71.42**	**80.95**	**61.90**	40	40.66
	T^2	**66.66**	**57.14**	**52.38**	**61.90**	**71.42**	33.33	40
Hold-one MMWPCA	**Q**	47.61	**52.38**	**76.19**	**85.71**	**71.42**	**53.33**	46.66
	T^2	**80.95**	**71.42**	**61.90**	**66.66**	**71.42**	40	40

* The comparison is done for the 15 Faults.

It is shown in Table 4.9 that the MMWPCA (hold-one and hold-five) and the MMW-DPCA with FLF record 0 % FAR for the training and testing data-sets. These results illustrate the high potentials of the developed monitoring schemes in terms of reducing FAR. Rato et al [33], Yu and Khan [118] and Wang et al [56] have not reported the FAR for those data-sets.

The MDR of the MMWPCA and the MMW-DPCA with FLF are presented in Table 4.10. The bold values highlight the best performance of the methods. The overall performance is indicated by the Mean MDR (MMDR) from which it can been seen that the overall

performance by the Q of the hold-one MMWPCA with FLF is better than the overall performance of the PCA [58], DPCA, MWPCA, RPCA, NGSSM, NDPCA and the LPPLS. The hold-one MMWPCA with FLF reduces also the MMDR by the T^2 compared to the all methods except for the NGSSM [118]. The hold-five MMWPCA with FLF results smallest values of the MMDR by both the Q and T^2 compared to all other methods. The same conclusion is drawn for the MMW-DPCA with FLF. For detailed comparison, consider the Table 4.12 that represents the percentage of the faults that have been detected with small MDR by the MMWPCA and the MMW-DPCA with FLF techniques compared against the methods presented in table 4.10. From this table, it is found that the hold-one MMWPCA with FLF detects more than 50% of the TEP faults by the T^2 better than PCA [58], DPCA [58], MWPCA [33], RPCA [33] and LPPLS while by the Q, it detects more 50% of TEP abnormalities with small MDR compared to the DPCA, MWPCA, RPCA, LPPLS and NGSSM. On the other hand, the hold-five MMWPCA with FLF detects more than 50% of the TEP faults better than all methods except the NGSSM and NDPCA via both monitoring indices. Based on the results of the Table 4.12, only the NGSSM method by the T^2 has shown a better MDR reduction compared to the MMW-DPCA with FLF based fault detection technique.

The detection delays obtained by the proposed methods are provided in the Table 4.11. The results are compared to the reported detection delays by Russell et al [58]. Wang et al [56], Rato et al [33] and Yu and Khan [118] did not report the detection delays. The hold-one MMWPCA with FLF reduces the detection delay for the faults 4, 6, 7, 9, 12, 15, 19, 20 and 21 via both monitoring indices. This factor is also reduced by the T^2 of this method for the faults 2, 8, 10, 11, 14, 16, 17 and 18. Both monitoring indices of the hold-five MMWPCA with FLF reduce the fault detection delay for the faults 9, 15, 19 and 21. In addition, faults 4 and 11 are detected earlier by its T^2. The Q and T^2 of the MMW-DPCA with FLF detect in a

short time delay the faults 2, 6, 9, 10, 11, 12, 15, 16, 17, 18, 19, 20 and 21. The MMW-DPCA with FLF decreases also the detection delay by the T^2 for faults 1, 4, 8, 13, and 14 while by the Q, this delay is reduced for faults 3 and 7.

Figures 4.7, 4.8, 4.9, 4.10 show the detection of the faults 5, 8, 13 and 16 by the hold-one MMWPCA with FLF respectively while the figures 4.11, 4.12, 4.13, 4.14 represent the detection of the faults 7, 10, 20 and 21 by the MMW-DPCA respectively [96, 100].

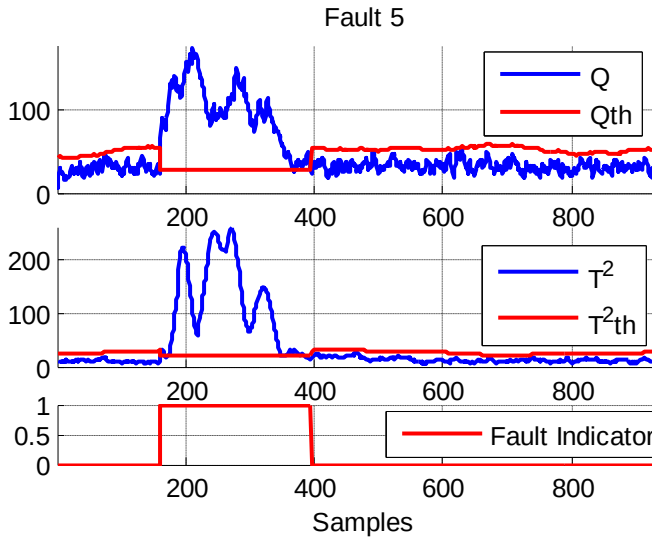

Figure 4.7. Detection of fault 5

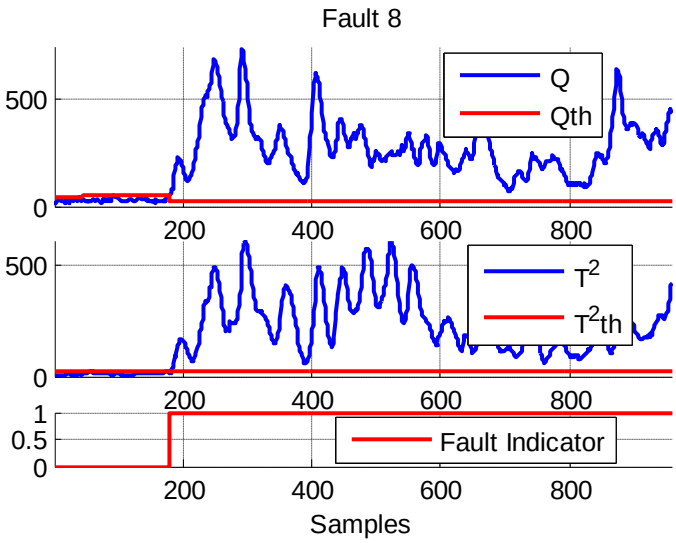

Figure 4.8. Detection of fault 8

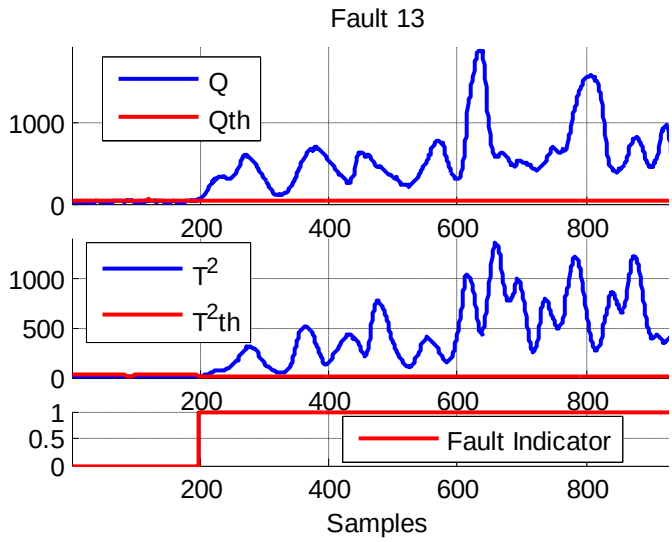

Figure 4.9. Detection of fault 13

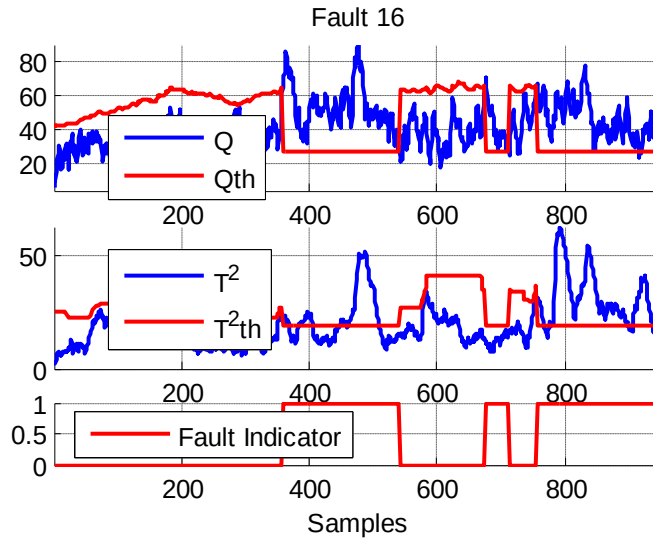

Figure 4.10. Detection of fault 16

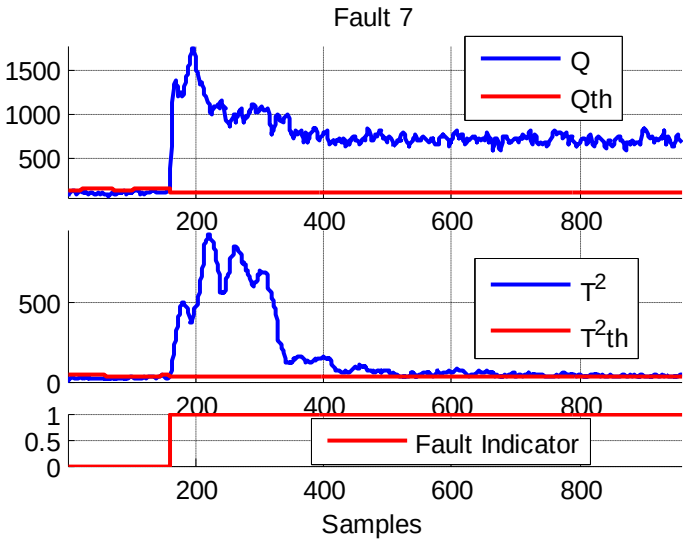

Figure 4.11. Detection of fault 7

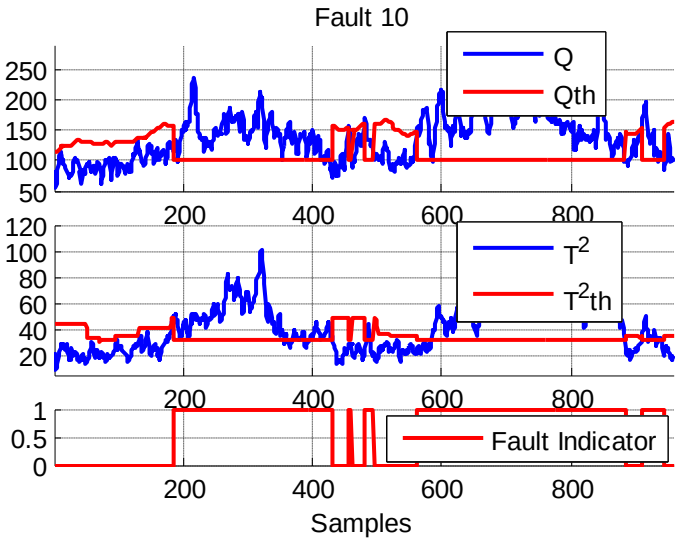

Figure 4.12. Detection of fault 10

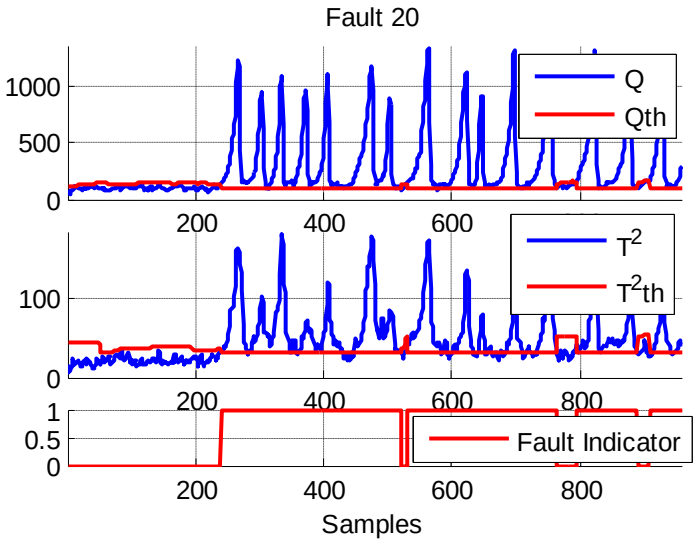

Figure 4.13. Detection of fault 20

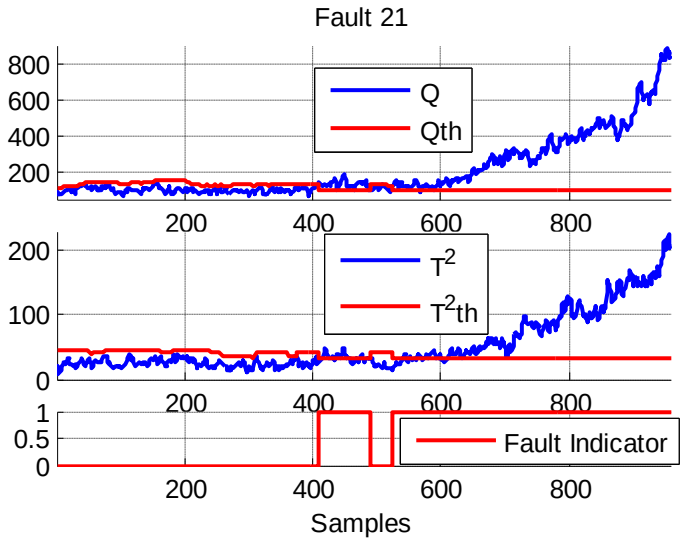

Figure 4.14. Detection of fault 21

4.2.3. Application of MMWPCA with FLF to the Revised TEP Model

The training data-set of the revised model has 83 measured variables and 1440 samples while the testing data-sets are of 83 variables and 10000 observations. The sampling interval is 3 minutes in each data-set. The faults are introduced at the sample 2000. The initial thresholds and the adaptive thresholds of the MMWPCA with FLF based fault detection technique are evaluated for 99% CL. Using parallel analysis criterion, 23 PCs are retained. These PCs explain 48.28% of the total variance in the training data-set. The moving window length and the FLF parameters are determined such that minimum FAR results in the testing

data-set (Fault 0). The method leads to 0% FAR in both the training and testing data-sets. These results signify that the detection accuracy is improved. The Fault Detection Rates (FDR) obtained for the TEP faults are given in Table 4.13. The FDR and the Mean FDR (MFDR) are compared against the values reported by Zhu et al [21], Rato et al [55], and Ciabattoni et al [119]. The bold values highlight the best performances [99].

Table 4.13. FDR (%) and MFDR (%) for the 24 Faults

Method	**The Proposed Method With FLF**		**Zhu et al [21]**	**Rato et al [55]**				**Ciabattoni et al [119]**
Statistics	**Q**	**T^2**	**PFI**	**T^2-SET-STA-MK**	**T^2-SET-STA-NM**	**T^2-SET-DYN-MK**	**T^2-SET-DYN-NM**	**SLR**
Fault No	**Fault Detection Rate (FDR%)**							
1	99.84	99.84	99.0	99.81	99.81	97.60	97.60	**99.94**
2	99.09	99.08	95.7	99.44	99.40	85.77	85.77	**99.5**
3	**100**	**100**	06.6	01.19	00.54	00.31	00.31	04.75
4	**100**	**100**	99.9	99.98	99.98	99.98	99.98	100
5	**100**	**100**	04.3	01.23	00.79	00.37	00.37	01.06
6	**100**	**100**	99.7	99.86	99.86	99.86	99.86	14.99
7	**100**	**100**	99.9	99.98	99.98	99.98	99.98	100
8	97.54	97.54	89.3	**99.10**	**99.08**	19.87	19.87	98.94
9	**99.23**	**99.21**	19.0	03.85	01.75	00.29	00.29	04.87
10	**99.02**	**99.01**	87.3	91.63	93.13	58.70	58.70	91.38
11	**99.84**	**99.84**	98.0	98.60	98.46	76.98	76.98	97.88
12	**99.62**	**99.62**	58.9	36.39	34.74	00.40	00.40	48.59
13	**96.48**	**96.48**	95.0	96.13	96.23	73.59	73.59	92.57
14	99.91	99.91	98.9	99.90	99.88	96.50	96.50	**99.94**
17	99.08	96.47	85.4	**99.60**	**99.60**	83.96	83.96	99.38
18	**95.61**	**95.61**	64.0	82.40	81.09	75.88	75.88	80.07
19	**99.72**	**99.72**	95.4	99.27	99.27	62.20	62.20	97.81
20	97.32	88.58	83.9	97.21	97.21	72.40	72.40	**98.13**
21	**99.75**	**99.75**	07.30	00.48	0.52	00.46	00.46	01.56
22	**99.78**	**99.77**	11.0	01.71	01.00	00.27	00.27	10.37
24	**99.61**	**99.58**	88.7	98.17	98.19	31.37	31.37	97.06
26	87.61	72.58	**91.3**	82.48	81.05	04.71	04.71	72.70
27	88.52	63.68	**92.3**	83.30	81.86	17.18	17.18	74.58
28	**06.43**	02.40	03.6	00.81	00.58	00.42	00.42	02.56
MFDR(%)	**94.33**	**92.02**	69.76	69.68	69.33	48.29	48.29	66.19

From this table, it can be seen that the MMWPCA with FLF provides better FDR compared to the one recorded by Rato et al [55] within the monitoring indices T^2-SET-STA-MK and T^2-

SET-STA-NM for all the faults except for the faults 8 and 17. Moreover, high FDRs are obtained when comparing the proposed method's Q and T^2 with T^2-SET-DYN-MK and T^2-SET-DYN-NM.T. Comparing to the method of Zhu et al [21], presented by the PFI statistic, the developed technique improves the FDR by both monitoring indices for all the TEP changes except for the faults 26 and 27. It can be demonstrated by the Table 4. 13 that the FDR of the SLR is slightly high compared to the one of the MMWPCA with FLF just for the faults 1, 2, 14 and 20. The MFDR gives the general performance of the methods. The MFDR of the proposed method is high compared to the one of the offered fault detection technique in the Table 4.13. These results reveal the effectiveness and the high performance potential of the monitoring proposal [99].

The detection of the faults 10, 14, 19, and 13 are depicted in the figures 4.15, 4.16, 4.17 and 4.18 respectively [99].

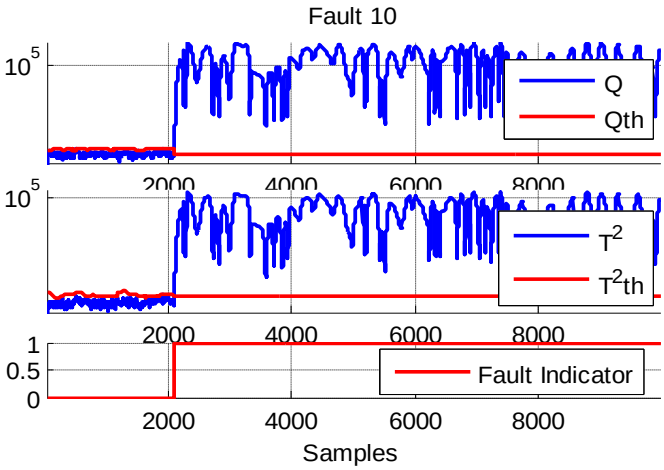

Figure 4.15. Detection of random variation

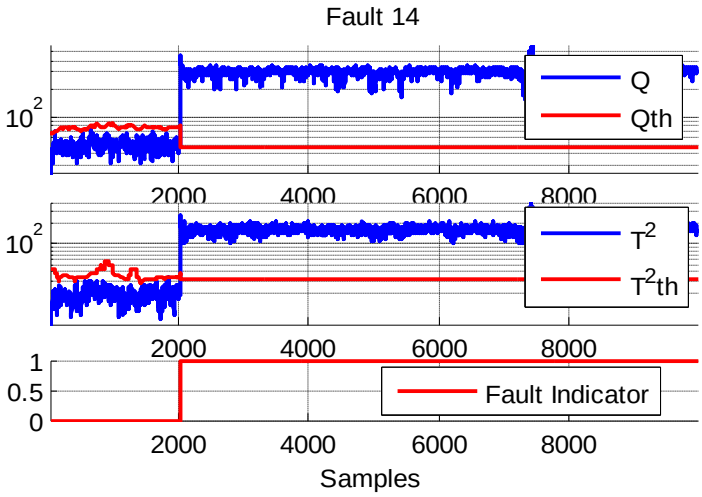

Figure 4.16. Detection of sticking

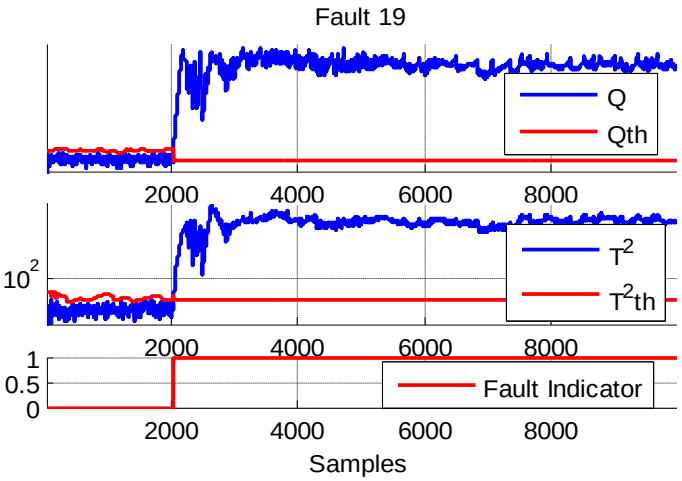

Figure 4.17. Detection of unknown fault

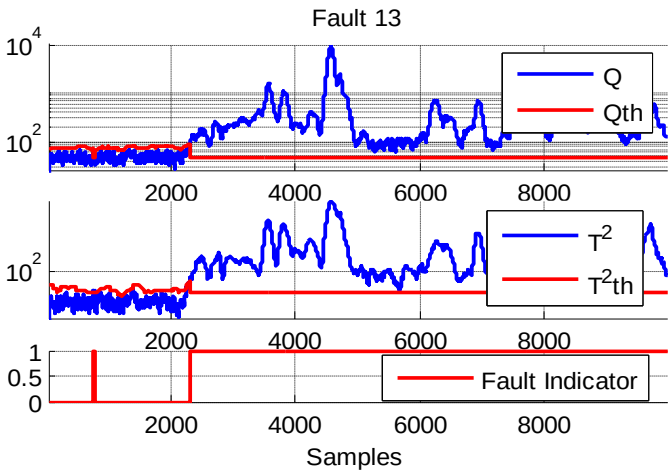

Figure 4.18. Detection of slow drift

4.2.4. Application of MMWPCA with FLF to the Cement Rotary Kiln

The MMWPCA with FLF has been applied to detect and identify a real fault of the cement rotary kiln. The data descriptions for this application are shown in the Table 4.14 [97].

Table 4.14. Different Data-Sets

Data set	Number of observations	Number of variables	Sampling time (sec)
Training data-set	482	51	30
Testing data-set	7900	51	1
Simulated faults data-set	2101	51	1
Faulty data-set	3286	51	1

The training data-set is utilized to construct the PCA model. The initial thresholds and the adaptive thresholds are computed for 99% CL. To validate the model, choose the window length and the FLF parameters, the testing data-set is used. Setting the CPV at 90%, 27 of PCs are retained. The length of the moving window is determined for minimum FAR is the testing data-set. Figure 4.19 represents how this window size is selected. According to this figure, the length is found to be 343. It corresponds to 0% FAR. The monitoring indices along with their adaptive thresholds for the training and testing data-sets are shown in the Figure 4.20. No false alarms are signaled for these two data-sets by the MMWPCA with FLF [97].

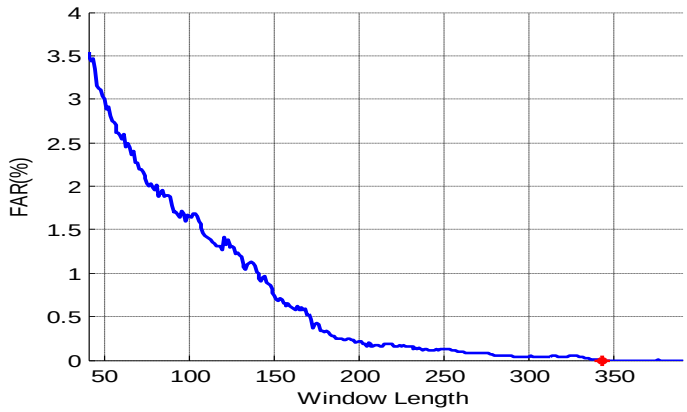

Figure 4.19. FAR versus the window length

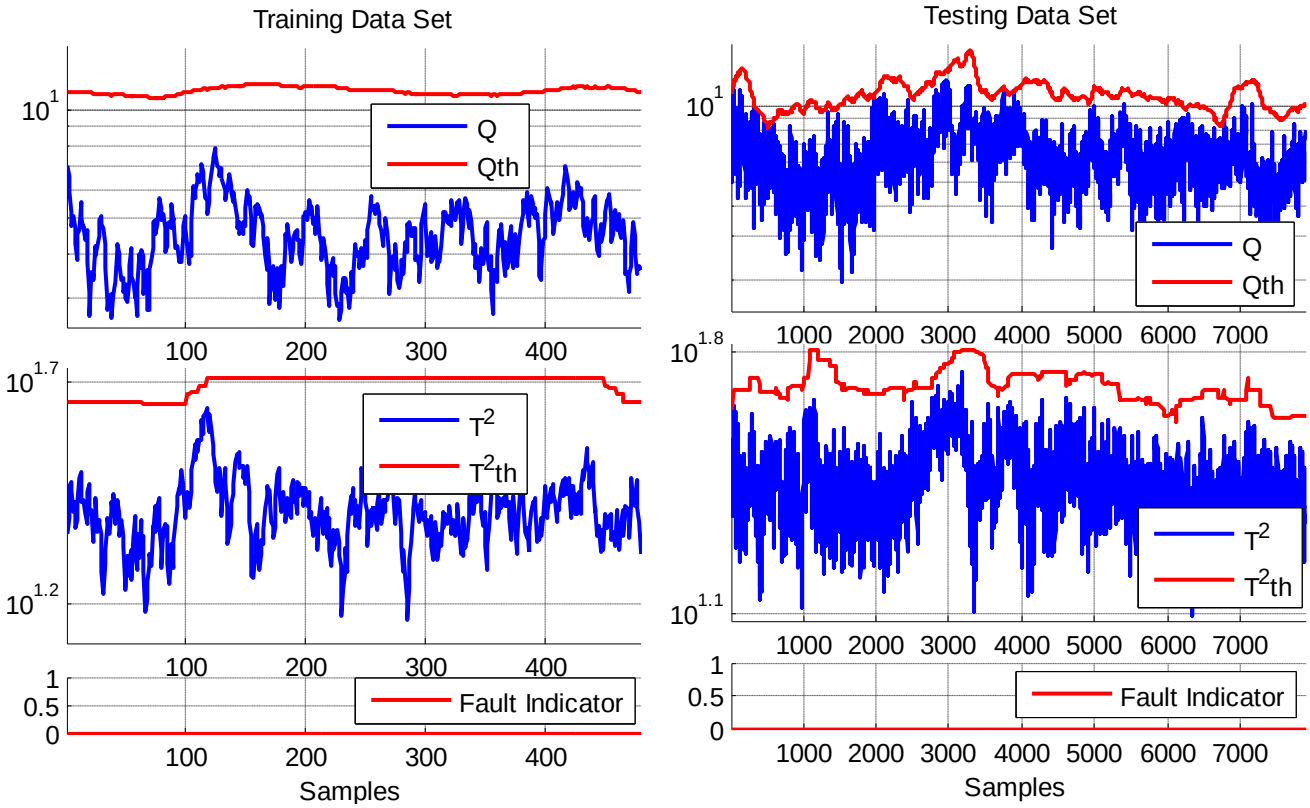

Figure 4.20. The monitoring indices with their associated thresholds for the training and the testing data-sets

The detection and identification accuracies of the MMWPCA with FLF have been tested first on simulated sensors faults before the method is applied to detect and identify the real fault. The simulated faults are described in the Table 4.15 [97].

Table 4.15. Simulated Faults

Sensor fault	Fault Description	Number of faulty samples	Fault amplitude
Fault 1	A Single abrupt fault activated at sample 1000 in the sensor number 20	200	+2%
Fault 2	Multiple abrupt fault activated at sample 1000 in the sensors number 5,8,12	200	+2%
Fault 3	Intermittent fault with variable amplitude started at 1000 in the sensor number 28	400	+3%,-1.5%, -2%,+2%
Fault 4	Single ramp fault activated on the sensor number 2 at sample 1000 with slop of 10^{-4}	500	From (0% to 5%)
Fault 5	Multiple ramp faults activated on sensors number 1, 3 ,4 sample 1000 with slop of 10^{-4}	500	From (0% to 5%)
Fault 6	Additive random noise fault with 0 mean and 0.05 standard deviation activated on sensor 50 at sample 10^3	300	Between -15% and 17%

The FAR, FDR and the detection time delay of each fault are tabulated in Table 4.16.

Table 4.16. FAR, FDR and the Detection Time Delay for the Simulated Faults

Simulated Fault	False Alarms Rate (FAR %)		Fault Detection Rate(FDR%)		Fault Detection Delay(s)	
Statistics	**Q**	**T^2**	**Q**	**T^2**	**Q**	**T^2**
Fault 1	0	0	100	99.5	0	1
Fault 2	0	0	100	99.5	0	1
Fault 3	0	0	99.2	98.7	0	1
Fault 4	0	0	89.4	94.6	48	27
Fault 5	0	0	90.8	90.8	46	46
Fault 6	0	0	100	99.6	0	1

According to this table, all the faults have been detection with 0% FAR. These results demonstrate the detection accuracy enhancements. The MMWPCA with FLF detects faults 1, 2, and 6 with 100% FDR and 0 sec delay by the Q whereas the detection is delayed by 1 sec via the T^2. No detection delay is introduced by the Q for the fault 3 but the FDR is not 100%. The relative high detection delays of the fault 4 and 5 are due to slops of the ramp faults which are taken very small. In general, all the simulated faults are detection with 0% FAR, high FDR and in a short detection delay [97].

The fault identification is performed through the use of the contribution plots. The variables with high contribution to the monitoring indices are identified as the variables responsible of the out of control status. Table 4.17 presents the variables at which the deviations are introduced and the identified ones. According the results, the identification of the fault source is very accurate [97].

Table 4.17. Fault Identification

Faults	Faulty Variables	Identified variables by	
Statistics	**/**	**Q**	**T^2**
Fault 1	x_{20}	x_{20}	x_{20}
Fault 2	x_5, x_8, x_{12}	x_5, x_8, x_{12}	x_5, x_8, x_{12}
Fault 3	x_{28}	x_{28}	x_{28}
Fault 4	x_2	x_2	x_2
Fault 5	x_1, x_3, x_4	x_1, x_3, x_4	x_1, x_3, x_4
Fault 6	x_{50}	x_{50}	x_{50}

The detection of the fault 1 and its corresponding contribution plots are depicted in Figure 4.21.

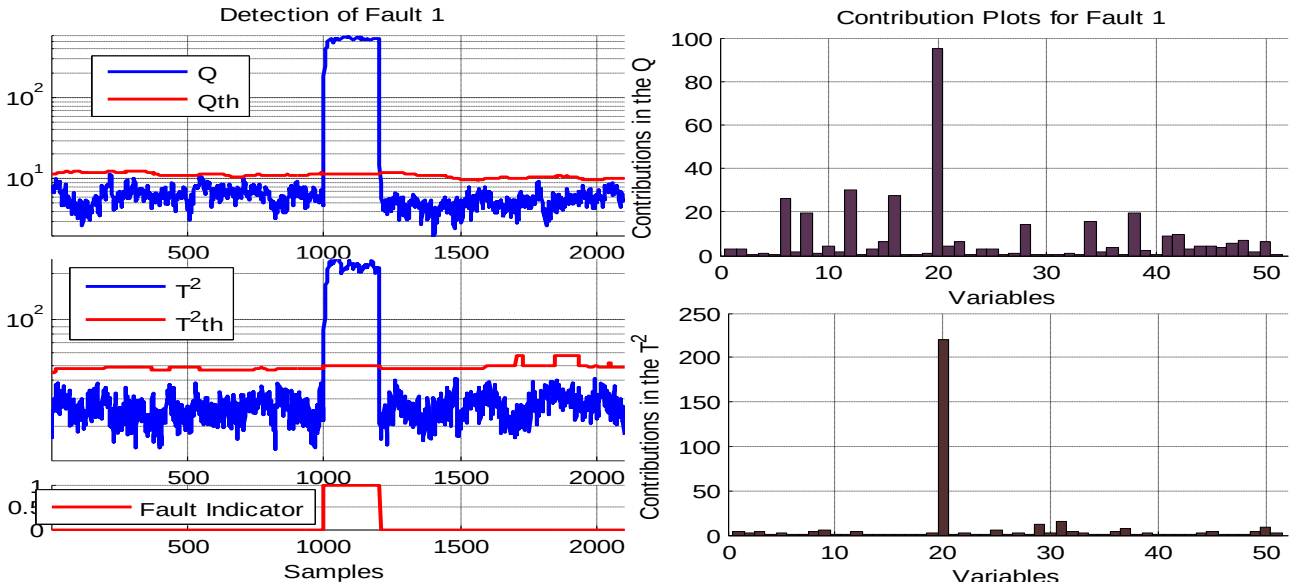

Figure 4.21. In the left: Q, T^2 and the thresholds. In the right: the variables contribution plots for fault 1

The application of the MMWPCA with FLF to the faulty data-set of the Table 4.14 allows the detection and identification of the real occurred fault in the CRK. The obtained results are shown in the Figure 4.22. This real fault has been successfully detected with no false alarm. The variables behind the faulty status are identified through the contribution plots.

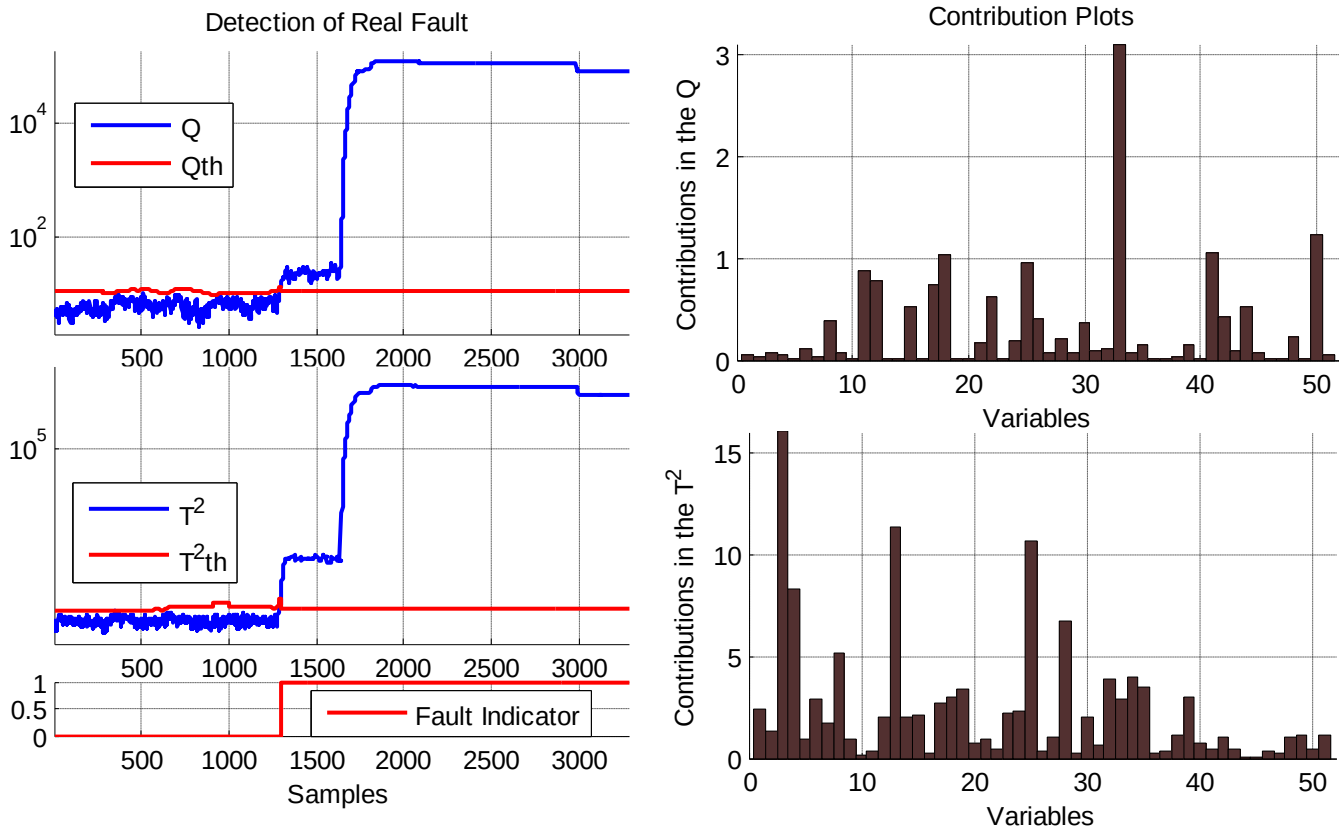

Figure 4.22. In the left: Q, T^2 and the thresholds. In the right: the variables contribution plots for the real fault

Referring the variables contribution to the monitoring indices in the Figure 4.22, the occurred fault is a multiple abnormality where several variables are involved. To better understanding the cause, one can consider the recorded error in the specified variables. Figure 4.23 displays those errors [97].

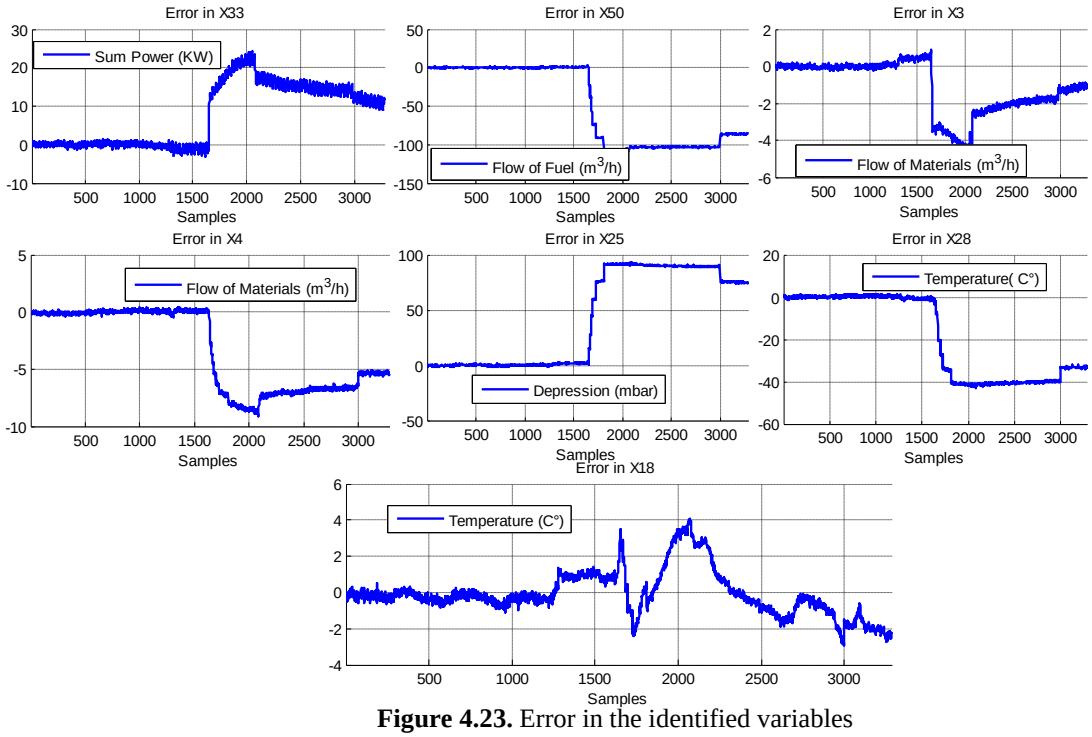

Figure 4.23. Error in the identified variables

The operator noticed that the production rate had been decreased. To overcome this problem, he started increasing the kiln's inputs, x_3 and x_4. But he made the system unstable by adding quantities more than the designed conditions. Consequently, the kiln's power (x_{33}), the gas outlet of the smoke box (x_{18}) and cyclone IV gas outlet (x_{28}) destabilized. The operator reduced abruptly the flow of materials entering the kiln from both tower I and II (x_3 and x_4) as a counteraction to this situation. This counteraction increased the temperature of gases in the outlet of smoke box of tower I (x_{18}). In addition, the rotation speed decreased to avoid the kin big shilling abnormality. In this case, the rotary kiln system must be restarted that is why the operator lowered the fuel rate to the main burner (x_{50}) [97].

4.2.5. Application of MMWPCA with FLF to the Grid-Connected Photovoltaic System

The fault detection in the Grid-Connected Photovoltaic System (GCPVS) is performed by measuring 29 variables. The PCA model of the MMWPCA with FLF is constructed based on a training data-set of 2766 observations. The model is validated using a testing data-set of 1500 samples. After the selection of all needed parameters of the proposed method, it is tested using sensor faults shown in the Table 4.18. The faulty data, which include the real fault, consists of 2465 samples. All the data-sets are sampled every 5 minutes. The length of the sliding window is found to be 142 [98].

Table 4.18. Simulated Faults

Faults	Fault Description	Number of Faulty Samples	Fault Amplitude
Fault 1	Abrupt fault activated at sample 600.	200	+1%
Fault 2	Additive random noise fault with 0 mean and 0.05 standard deviation activated at sample 10^3.	300	Between -15% and 17%
Fault 3	Ramp fault activated at sample 700 with slop of 1.5×10^{-4}.	500	From (0% to 9%)

The monitoring indices with the adaptive thresholds for the training and testing data-sets are depicted in the following figures [98].

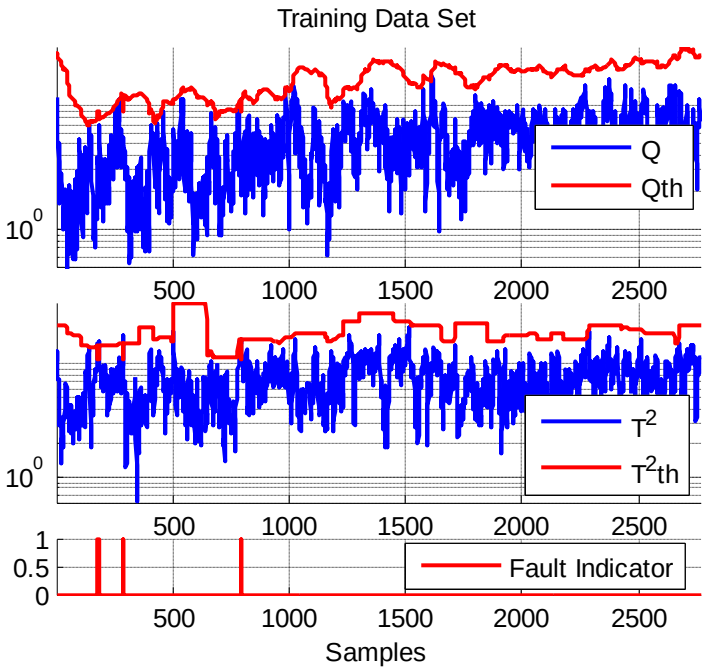

Figure 4.24. Training data-set

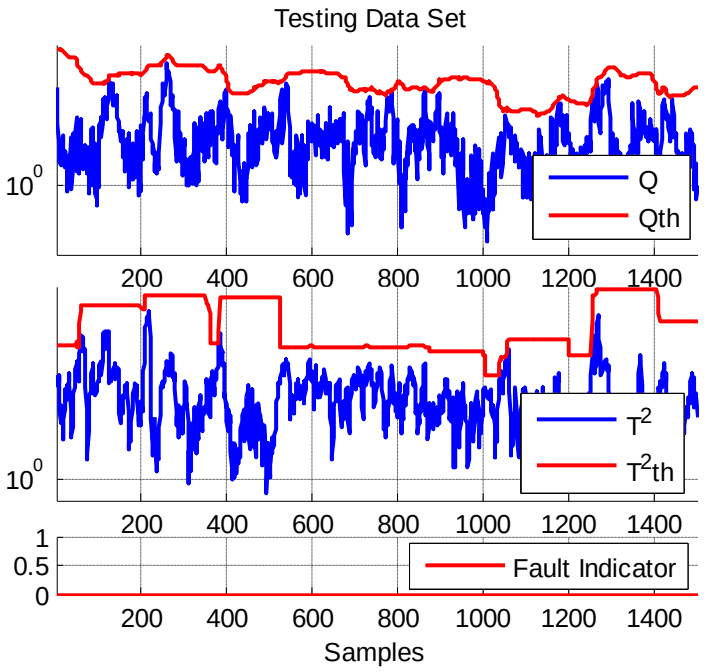

Figure 4.25. Testing data-set

According to the Figure 4.24, some false alarms are signaled in the T^2 statistic. These false alarms correspond to 0.61% FAR which is negligible. In the Figure 4.25, it can be seen clearly that no false alarm is recorded for the testing data-set [98].

The detections of the simulated faults are depicted in Figures 4.26, 4.27 and 4.28 [98].

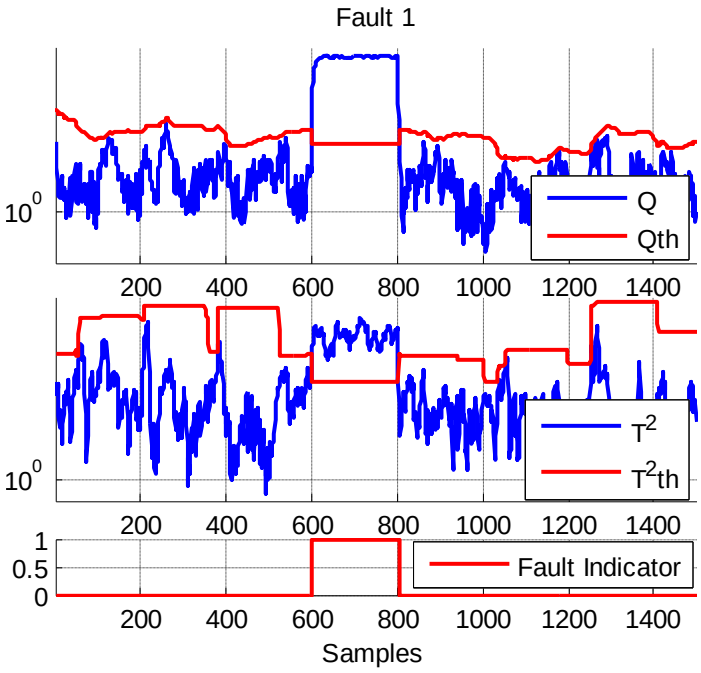

Figure 4.26. Detection of abrupt fault

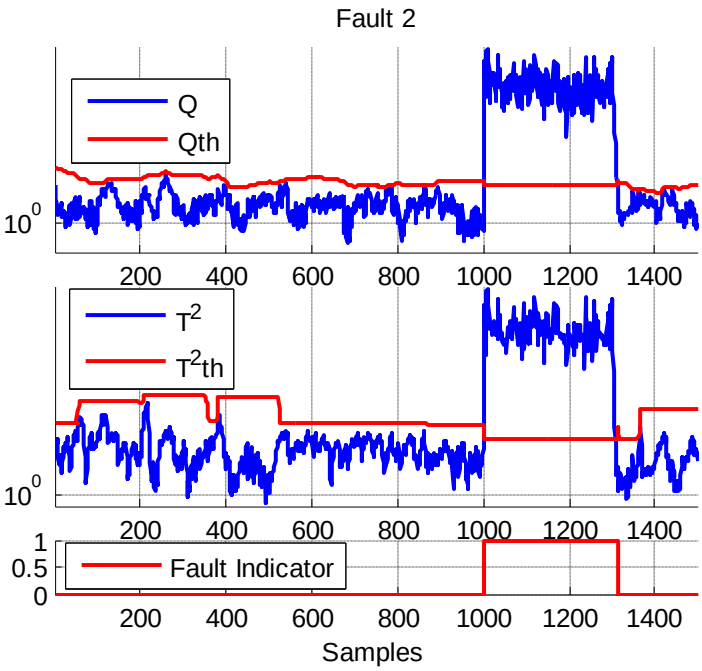

Figure 4.27. Detection of random fault

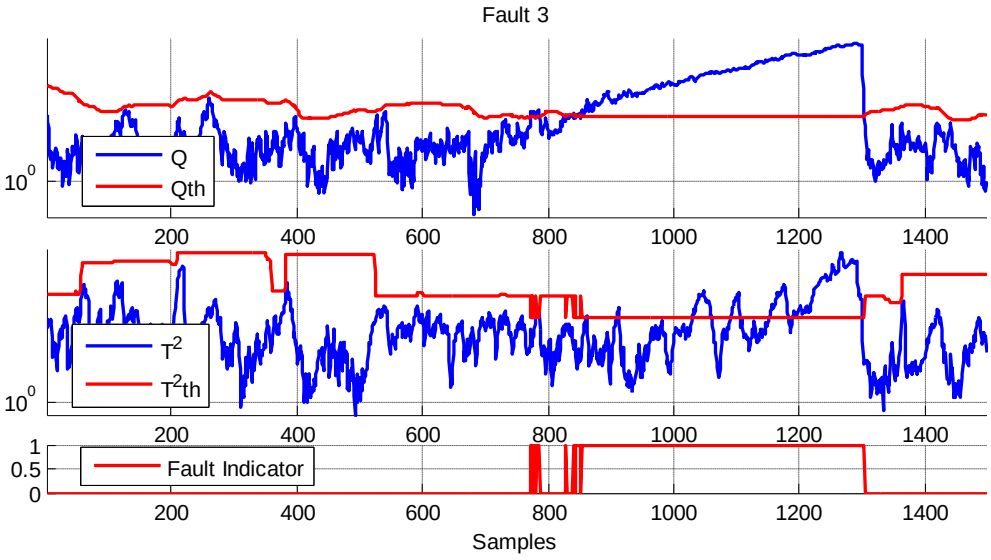

Figure 4.28. Detection of ramp fault

Figure 4.26 and 4.27 illustrate that the detection of the simulated faults is exactly at the occurrence time of each fault. The detection of the ramp fault is delayed because the used slop is very small. After this test, the MMWPCA with FLF is applied to real faulty data. The results are shown in the Figure 4.29. Since no false alarms are recorded by the Q statistic for the training data-set and no false alarm is also signaled by the MMWPCA with FLF monitoring indices in the testing data-set, it can be concluded that any violation of the adaptive thresholds with high percentage can be considered as a fault. This is the case that is observed in the Figure 4.29, thus the real fault has been successfully detected [98].

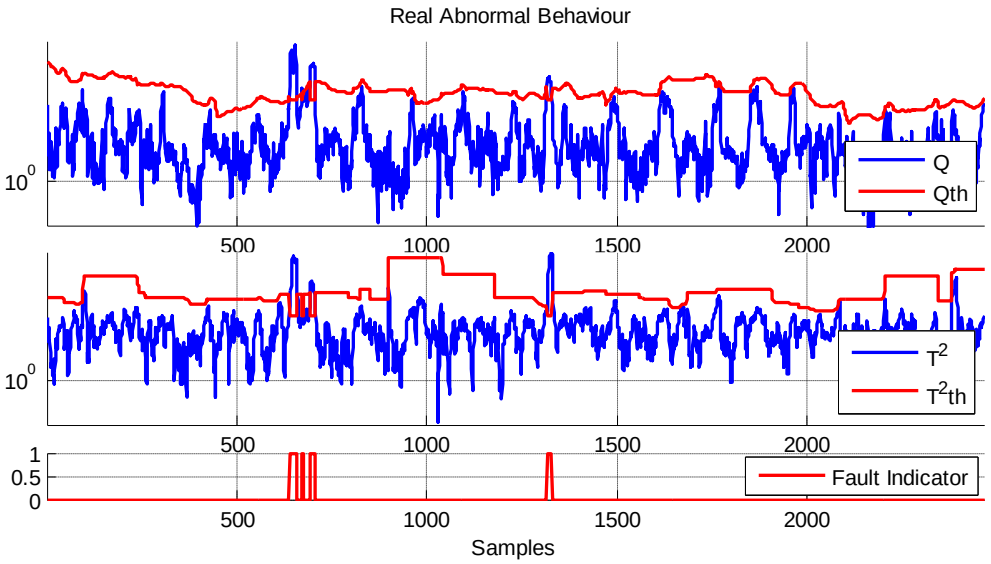

Figure 4.29. Detection of real fault

Chapter four summarizes the simulation and the experimental results of the proposed methods on the different processes. The CFAR method reduces the effect of the false alarms in process monitoring and detects successfully all the types of faults. However it has a main drawback that is undesirable in the fault detection and diagnosis field. This drawback is the detection delay which is high for fast systems. This problem is encountered because the detection of faults by the CFAR method is done by accumulating the number of samples which are above the PCA monitoring indices thresholds. Hence, the accumulated sum needs a time to exceed the CFAR thresholds.

The MMWPCA with FLF showed high detection performance in either the TEP or in the CRK and the GCPVS. It reduces the FAR, MDR and the detection time delay. It improves also the PCA performance in process monitoring. The adaptive thresholds of this method increase the sensitivity of the monitoring indices leading to enhancements in the FDR. The FLF involves also in the FDR improvements and in the FAR reduction. As it is demonstrated through the comparison results against recent published papers, the MMWPCA with FLF showed high potential in terms of the average MDR or FDR. The scheme performance has been proved by the real application to the CRK and GCPVS where the real occurred faults in the systems have been successfully detected. The fault identification of the proposed technique is also very accurate as it is illustrated by the sensors faults in the CRK data.

The MMW-DPCA with FLF is the dynamic extension of the MMWPCA with FLF where the dynamic behaviors are included in the PCA model. This monitoring scheme showed also high detection performance compared to recent works in the fault detection and diagnosis area. It enhances the DPCA based fault detection method by means of the adaptive thresholds and the FLF that ensures robustness to noise and outliers. This method also has been applied to the CRK where the real fault has been successfully detected. The results are presented and discussed in [100].

Conclusion

Conclusion

The performance of any monitoring scheme relies on the reduction of the False Alarm Rate (FAR), Missed Detection Rate (MDR) and Detection Time Delay (DTD). The more these criteria are reduced, the more efficient the monitoring scheme is. The problems encountered with MSPC motivated many researchers to enhance process monitoring in order to achieve accurate fault detection and in a short DTD.

Throughout this thesis, several techniques have been proposed to reduce FAR, MDR and the DTD. These techniques include Constant False Alarms Rate (FAR), Modified Moving Window PCA (MMWPCA) and Modified Moving Window Dynamic PCA (MMW-DPCA) with FLF. The CFAR technique, as it has been demonstrated in the applications part, reduces the FAR and accomplishes the detection of a real process fault with high accuracy and with no false alarms; however, this methods needs some additional improvements to reach satisfactory process monitoring performances. Hence, as a future work, it is proposed to apply this technique with adaptive thresholding schemes to reduce the detection delays and improve the FDR. It has been also illustrated through the applications that the MMWPCA and MMW-DPCA with FLF provide high detection potentials and performances better than the methods which have been recently proposed in the field of FDD. The use of the FLF shows an interesting performance when it is combined with data-driven techniques. It has been used in the goal of ensuring spikes elimination in the monitoring indices for more accurate detection without introducing a delay in the abnormality detection.

MMWPCA with FLF based monitoring scheme enhances the monitoring performance by combining the advantages of both PCA and MWPCA based fault detection methods. Both adaptive thresholds and the FLF improve the PCA performance. Furthermore, this technique has been extended to MMW-DPCA with FLF to handle the dynamic behaviour in the data.

This dynamic extension improves the performance of DPCA in the fault detection with a simple dynamic structure. The adaptive thresholds of these techniques do not require updating the statistical model to be generated.

Industrial systems are generally nonlinear processes; thus, to deal with the nonlinear behaviours, one can extent the proposed methods to a Modified Moving Window Kernel PCA (MMW-KPCA) with FLF. Both the dynamics and nonlinearities of the data can be handled by developing a Modified Moving Window Dynamic Kernel PCA (MMW-DKPCA) with FLF in which the statistical model will include both the dynamic and nonlinear characteristics; hence, data-driven methods in process monitoring can be improved further via these two techniques.

References

References

[1] M. M. Rashid, J. Yu. A new dissimilarity method integrating multidimensional mutual information and independent component analysis for non-Gaussian dynamic process monitoring. Chemometrics and Intelligent Laboratory Systems. 115 (2012) 44–58.

[2] X. Zhang, M. Kano, Y. Li. Locally weighted kernel partial least squares regression based on sparse nonlinear features for virtual sensing of nonlinear time-varying processes. Computers and Chemical Engineering. 104 (2017) 164–171.

[3] X. Deng, X. Tian, S. Chen. Modified kernel principal component analysis based on local structure analysis and its application to nonlinear process fault diagnosis. Chemometrics and Intelligent Laboratory Systems. 127 (2013) 195–209.

[4] Q. Jiang, X. Yan. Weighted kernel principal component analysis based on probability density estimation and moving window and its application in nonlinear chemical process monitoring. Chemometrics and Intelligent Laboratory Systems.127 (2013) 121–131.

[5] K. Liu ,Z. Fei, B. Yue, J. Liang, H. Lin. Adaptive sparse principal component analysis for enhanced process monitoring and fault isolation. Chemometrics and Intelligent Laboratory Systems. 146 (2015) 426–436.

[6] Y. Zhang., Y. Zhang. Fault detection of non-Gaussian processes based on modified independent component analysis. Chemical Engineering Science. 65(2010) 4630–4639.

[7] C. Zhao, F. Gao, Online fault prognosis with relative deviation analysis and vector autoregressive modeling. Chemical Engineering Science, 138(2015) 531-543.

[8] F. Harrou, F. Kadri, S.Chaabane, C. Tahon, Y. Sun. Improved principal component analysis for anomaly detection: Application to an emergency department. Computer & Industrial Engineering. 88 (2015) 63–77.

[9] F. Harrou, M. Madakyaru, Y. Sun, , S. Khadraoui. Improved detection of incipient anomalies via multivariate memory monitoring charts: Application to an air flow heating system. Applied Thermal Engineering.109 (2016) 65–74.

[10] K. P. Detroja, R. D. Gudi, S. C. Patwardhan, K. Roy. Fault detection and isolation using correspondence analysis. Ind. Eng. Chem. Res. 45 (2006) 223-235.

[11] C. Sumana , K. Detroja , R. D.Gudi, Evaluation of nonlinear scaling and transformation for nonlinear Process fault detection, Int J Adv Eng Sci Appl Math. 4 (2012) 52–66.

[12] S. Yin, S. X. Ding, X. Xie, H. Luo. A Review on Basic Data-Driven Approaches for Industrial Process Monitoring. IEEE Transactions on Industrial Electronics. 61 (2014) 6418-6428.

[13] A. Miao, Z. Ge, Z. Song, L. Zhou. Time neighborhood preserving embedding model and its application for fault detection. Ind. Eng. Chem. Res. 52, (2013) 13717 −13729.

[14] S. J. Qin. Survey on data-driven industrial process monitoring and diagnosis. Annu. Rev. Control. 36, (2012) 220 −234.

[15] J. MacGregor, A. Cinar. Monitoring, fault diagnosis, fault −tolerant control and optimization: data driven methods. Comput. Chem. Eng. 47 (2012) 111 −120.

[16] Z. Ge, Z. Song, F. Gao,. Review of recent research on data-based process monitoring. Ind. Eng. Chem. Res. 52 (2013) 3543 −3562.

[17] M. A. Atoui, S. Verron, A. Kobi. Fault detection with Conditional Gaussian Network. Engineering Applications of Artificial Intelligence. 45 (2015) 473–481.

[18] H. Fei, X. Jinwu. A novel process monitoring and fault detection approach based on statistics locality preserving projections. Journal of Process Control. 37 (2016) 46–57.

[19] D. Aguado, T. Montoya, L. Borras, A. Seco, J. Ferrer. Using SOM and PCA for analysing and interpreting data from a P-removal SBR. Engineering Applications of Artificial Intelligence. 21 (2008) 919–930.

[20] E. B. Martin, A .J. Morris, J. Zhang. Process performance monitoring using multivariate statistical process control. Systems Engineering for Automation, IEE Proc -Control Theory Appl. 143 (1996) 132-144.

[21] J. Zhu, Z. Ge, Z. Song. Distributed parallel PCA for modeling an monitoring of large-scale plant-wide processes with big data. IEEE Trans. Ind. Informat. 13 (2017) 1877-1885.

[22] Z. Ge, J. Chen. Plant-wide industrial process monitoring: A distributed modeling framework. IEEE Trans. Ind. Informat. 12 (2016) 310-321.

[23] J. Yu. Process monitoring through manifold regularization-based GMM with global/local information. Journal of Process Control. 45 (2016) 84–99.

[24] B. Wang, X. Yan, Q. Jiang, Z. Lv. Generalized Dice's coefficient-based multi-Block principal component analysis with Bayesian inference for plant-wide process monitoring. Journal of Chemometrics. DOI:10.1002/cem.2687.

[25] Q. Jiang, B. Huang, X. Yan. GMM and optimal principal components-based Bayesian method for multimode fault diagnosis. Computers and Chemical Engineering. 84 (2016) 338–349.

[26] E. Cai, D. liu, L. Liang, G. Xu, Monitoring of chemical industrial processes using integrated complex network theory with PCA. Chemometrics and Intelligent Laboratory Systems. 140 (2015) 22–35.

[27] J. Ramahaleomiarantsoa, N. Heraud, E. J. R. Sambatra, J. M. Razafimahenina, On the Sensitivity of Principal Components Analysis Applied in Wound Rotor Induction Machines Faults Detection and Localization. International Journal of Energy Science. 2 (2012) 262-271.

[28] Y. Dong, S. J. Qin. A novel dynamic PCA algorithm for dynamic data modeling and process monitoring. Journal of Process Control. (2017). doi: https://doi.org/10.1016/j.jprocont.2017.05.002.

[29] S. Gajjar, A. Palazoglu. A data-driven multidimensional visualization technique for process fault detection and diagnosis. Chemometrics and Intelligent Laboratory Systems. (2016). doi: 10.1016/j.chemolab.2016.03.027.

[30] S. W. Choi, E. B. Martin, A. J. Morris, I-B. Lee. Adaptive multivariate statistical process control for monitoring time-varying processes. Ind. Eng. Chem. Res. 45 (2006) 3108-3118.

[31] W. Ku, R. H. Storer, C. Georgakis. Disturbance detection and isolation by dynamic principal component analysis. Chemometrics and Intelligent Laboratory Systems. 30 (1995) 179-196.

[32] T. J. Rato, M. S. Reis.Fault detection in the Tennessee Eastman benchmark process using dynamic principal components analysis based on decorrelated residuals (DPCA-DR). Chemometrics and Intelligent Laboratory Systems. 125 (2013) 101-108.

[33] T. J. Rato, M. Reis, E.Schmitt, M. Hubert, B. De Ketelaere. A systematic comparison of PCA-based statistical process monitoring methods for high-dimensional, time-dependent processes. Process systems Engineering, AIChE. 62 (2016) 1478-1493.

[34] T. J. Rato, M. S. Reis, Defining the structure of DPCA models and its impact on process monitoring and prediction activities. Chemometrics and Intelligent Laboratory Systems. 125 (2013) 74–86.

[35] L. Ren, Z. Y. Xu, X. Q. Yan. Single-sensor incipient fault detection. IEEE Sensors J. 11(2011) 2102-2107.

[36] X. Deng, X. Tian, S.Chen, C. J. Harris. Fault discriminant enhanced kernel principal component analysis incorporating prior fault information for monitoring nonlinear processes. Chemometrics and Intelligent Laboratory Systems. 162 (2017) 21–34.

[37] J. Huang, X. Yan. Quality relevant and independent two block monitoring based on mutual information and KPCA. IEEE Trans. Ind. Electron. 64 (2017) 6518-6527.

[38] J-H. Cho, J-M. Lee, S. W. Choi, D. Lee, I-B. Lee. Fault identification for process monitoring using kernel principal component analysis. Chemical Engineering Science. 60 (2005) 279–288.

[39] J-M. Lee, C. Yoo, S. W. Choi, P. A. Vanrolleghem, I-B. Lee. Nonlinear process monitoring using kernel principal component analysis. Chemical Engineering Science. 59 (2004) 223–234.

[40] Q. Jiang, X. Yan. Nonlinear plant-wide process monitoring using MI-spectral clustering and Bayesian inference-based multiblock KPCA. Journal of Process Control 32 (2015) 38–50.

[41] L. Luo, S. Bao, Jianfeng Mao, D. Tang, Nonlinear process monitoring based on kernel global–local preserving projections. Journal of Process Control 38 (2016) 11–21.

[42] N. V. Ha, G. J-Claude. Fault detection based on kernel principal component analysis. Engineering Structures. (2010), doi: 10.1016/j.engstruct.2010.08.012.

[43] B. de Lázaro. J.M. Moreno, A.P. Santiago, O.L. da Silva, A.J. Neto. Optimizing kernel methods to reduce dimensionality in fault diagnosis of industrial systems. Computers & Industrial Engineering (2015), doi: http://dx.doi.org/10.1016/j.cie.2015.05.012.

[44] B. De Ketelaere, M. Hubert, E. Schmitt. Overview of PCA-based statistical process-monitoring methods for time-dependent, high-dimensional data. Journal of Quality Technology. 47 (2015) 328-335.

[45] Z. Mao, Y. Zhao, L. Zhou. A Flexible Principle Component Analysis Method for Process Monitoring. Fourth International Conference on Natural Computation. 2008, doi:10.1109/ICNC.2008.750.

[46] X. Wang, U. Kruger, G. W. Irwin. Process monitoring approach using fast moving window PCA. Industrial & Engineering Chemistry Research. 44 (2005) 5691-5702.

[47] S. Wold. Exponentially weighted moving principal components analysis and projections to latent structures. Chemometrics and Intelligent Laboratory Systems. 23 (1994) 149-161.

[48] W. Li, H. Yue, S. V. Cervantes, S. J. Qin. Recursive PCA for adaptive process monitoring. Journal of Process Control. 10 (2000) 471-486.

[49] L.M. Elshenawy, S. Yin, A. S. Naik, S. X. Ding. Efficient Recursive Principal Component Analysis Algorithms for Process Monitoring. Ind. Eng. Chem. Res. 49 (2010) 252−259.

[50] Y. Fan, W. Zhang, Y. Zhang. Monitoring of nonlinear time-delay processes based on adaptive method and moving window. Mathematical Problems in Engineering. (2014). http://dx.doi.org/10.1155/2014/546138.

[51] J. Ni, C. Zhang, S. X. Yang. An adaptive approach based on KPCA and SVM for real-time fault diagnosis of HVCBs. IEEE Trans. Power Del. 26 (2011) 1960-1971.

[52] R. Fazai, O. Taouali, M. F. Harkat, N. Bouguila. A new fault detection method for nonlinear process monitoring. Int J Adv Manuf Technol, 87 (2016) 3425-3436.

[53] X. Liu, J. M. Kennedy, D. M. Laverty, D. J. Morrow, S. McLoone. Wide-area phase-angle measurements for islanding detection—An adaptive nonlinear approach. IEEE Trans. Power Del. 31 (2016) 1901-1911.

[54] Z. Lou, D. Shen, Y. Wang,..Two-Step principal component analysis for dynamic processes monitoring. The Canadian Journal of Chemical Engineering. (2017), doi: 10.1002/cjce.22855.

[55] T. J. Rato and M. S. Reis. Markovian and Non-Markovian sensitivity enhancing transformations for process monitoring. Chemical Engineering Science. 163 (2017) 223-233.

[56] H. Yu, F. Khan, Improved latent variable models for nonlinear and dynamic process monitoring, Chemical Engineering Science. 168 (2017) 325-338.

[57] S. Wold, J. Trygg, A. Berglund, , H. Antti. Some recent developments in PLS modeling. Chemom. Intell. Lab. Syst. 58 (2001)131–150.

[58] E. L. Russell, L. H. Chiang, R. D. Braatz. Fault detection in industrial processes using canonical variate analysis and dynamic principal component analysis. Chemometrics and Intelligent Laboratory Systems, 51 (2000) 81–93.

[59] N. Zhong, X. Deng. Multimode Non-Gaussian process monitoring based on local entropy independent component analysis. (2016), doi: 10.1002/cjce.22651.

[60] J.F. Barragan, C.H. Fontes, M. Embiruçu,. A Wavelet-based clustering of multivariate time series using a multiscale SPCA approach. Computers & Industrial Engineering. 2016, doi: http://dx.doi.org/10.1016/j.cie.2016.03.003

[61] Y. Hu, T. Palmé, O. Fink. Fault detection based on signal reconstruction with Auto-Associative Extreme Learning Machines. Engineering Applications of Artificial Intelligence. 57 (2017) 105–117.

[62] E. C. Mid, V. Dua. Model-based parameter estimation for fault detection using multi-parametric programming. Ind. Eng. Chem. Res. 56 (2017) 8000–8015.

[63] R. Isermann. Fault-diagnosis systems an introduction from fault detection to fault tolerance. Springer, Germany. 2006.

[64] E. Sobhani-Tehrani, K. Khorasani. Fault diagnosis of nonlinear systems using hubrid approach. Chapter book, 21-49. doi: 10.1007/978-0-387-92907-1_2.

[65] L. H. Chiang, E. L. Russell, R. D. Braatz. Fault detection and diagnosis in industrial systems. Springer, London, 2001.

[66] V. Venkatasubramanian, R. Rengaswamy, K. Yin, S. N. kavuri. A review of process ault detection and diagnosis Part I: Quantitative model-based methods. Computers and Chemical Engineering. 27 (2003) 293-311.

[67] V. Venkatasubramanian. R. Rengaswamy, S.N, Kavuri. A review of process fault detection and diagnosis PartII qualitative models and research stratigies. Computers and Chemical Engineering. 27 (2003) 313-326.

[68] V. Venkatasubramanian, R. Rengaswamy, S. N. kavuri, K. Yin. A review of process fault detection and diagnosis PartIII Process history based methods. Computers and Chemical Engineering. 27 (2003) 327-346.

[69] T. Umeda, T. Kuriyama, E. Osghima, H. Matsuyamah. A graphical approach to cause and effect analysis of chemical processing ystems. Chem. Eng. Science. 35(1980) 2379 – 2388.

[70] S. Katipamula, M. R, Brambley. Methods for Fault Detection, Diagnostics, and Prognostics for Building Systems—A Review, Part I. 11 (2005) 3-25.

[71] R. Wang, J. Wang, , J. Zhou, H. Wu. Fault diagnosis based on the integration of exponential discriminant analysis and local linear embedding. The Canadian Journal of Chemical Engineering. (2017), doi: 10.1002/cjce.22921.

[72] Z. Gao, H. Saxen, C. Gao. Guest editorial special Section on data-driven approaches for complex industrial systems. IEEE Trans. Ind. Informat. 9 (2013) 2210 – 2212.

[73] S. Maleki, C. Bingham, Y. Zhang. Development and realization of change point Analysis for the detection of emerging faults on industrial systems. IEEE Trans. Ind. Informat, 12 (2016) 1180-1187.

[74] G. Li, S. J. Qin, D. Zhou. A new method of dynamic latent-variable modeling for process monitoring. IEEE Trans. Ind. Electron. 61(2014).

[75] E. Vanhatalo. Multivariate process monitoring of an experimental blast furnace. Quality and Reliability Engineering International. 26 (2010) 495-508.

[76] A. Das, J. Maiti, R.N. Banerjee. Process monitoring and fault detection strategies: a review. International Journal of Quality & Reliability Management. 29 (2012) 720 - 752 http://dx.doi.org/10.1108/02656711211258508.

[77] J. F. MacGregor, T Kourti. Statistical process control of multivariate processes. Control Eng. Practice. 3 (1995) 403- 414.

[78] T. Kourti, J. Lee, J. F. MacGregor. Experiences with industrial application of projection methods for multivariate statistical process control. Computers Chem. Engng. 20 (1996) 745-750.

[79] S. Bao, L. Luo, J. Mao, Di Tang. Improved fault detection and diagnosis using sparse global-local preserving projections. Journal of Process Control. 47 (2016) 121–135.

[80] P.C. Deng, W.H. Gui, Y.F. Xie. Latent space transformation based on principal component analysis for adaptive fault detection. IET Control Theory and Appl 4 (2010) 2527 – 2538.

[81] C. Giannetti, R.S. Ransing, M. R. Ransing, C. D. Bould, D. T. Gethin, J. Sienz. A novel variable selection approach based on co-linearity index to discover optimal process settings by analysing mixed data. Computers & Industrial Engineering 72 (2014) 217–229.

[82] A. Giantomassi, F. Feeracuti, S. Larlori, G. Ippoliti, S. Longhi. Electric motor fault detection and diagnosis by kernel density estimation and kullback-leibler divergence based on stator current measurements. IEEE Trans. Ind. Electron 62 (2015) 1770-1780.

[83] J. C.-H. Pan, D. HE. Tai. A new strategy for defect inspection by the virtual inspection in semiconductor wafer fabrication. Computers & Industrial Engineering. 60 (2011) 16–24.

[84] B. Mnassri, E. M. El Adel, M. Ouladsine. Analysis and comparison of an improved unreconstructed variance criterion to other criteria for estimating the dimension of PCA model. Journal of Process Control 44. (2016) 207–223.

[85] M. Z. Sheriff, M. Mansouri, M. N. Karim, H. Nounou, M. Nounou. Fault detection using multiscale PCA-based moving window GLRT. Journal of Process Control 54(2017) 47–64.

[86] E. P. Tao, W. H. Shen, T. L. Liu, X. Q. Chen. Fault diagnosis based on PCA for sensors of laboratorial wastewater treatment process. Chemometrics and Intelligent Laboratory Systems. 128 (2013) 49–55.

[87] N. Basha, M. Nounou, H. Nounou, Multivariate fault detection and classification using interval principal component analysis, Journal of Computational Science (2018), https://doi.org/10.1016/j.jocs.2018.04.017.

[88] H. Ji, X. He, J. Shang, D. Zhou, Incipient sensor fault diagnosis using moving window reconstruction-based contribution, Ind. Eng. Chem. Res (2016), 10.1021/acs.iecr.5b03944.

[89] J. Xuan. Z. Xu. Y. Sun. Selecting the number of principal components on the Basis of Performance optimization of fault detection and identification. Ind. Eng. Chem. Res. 54 (2015) 3145-3153.

[90] I .Jaffel, O. Taouali, M. F. Harkat, H. Messaoud. Online process monitoring using a new PCMD index. Int J Adv Manuf Techno, 80 (2015) 947–957.

[91] A. Bakdi, A. Kouadri, A. Bensmail, Fault detection and diagnosis in a cement rotary kiln using PCA with EWMA-based adaptive threshold monitoring scheme. Control Engineering Practice. 66 (2017) 64–75.

[92] L. Guttman. Some necessary conditions for common factor analysis. Psychometrika. 19 (1954)149–161.

[93] H. Hotelling. Multivariate quality control illustrated by the testing of sample bombsights. In M. W. Hastay, W. A. Wallis, & C. Eisenhart (Eds.). Selected techniques of statistical analysis. New York: McGraw-Hill. (1947).

[94] J. E. Jackson, G. S. Mudholkar, Control Procedures for Residuals Associated With Principal Component Analysis, Technometrics. 21 (1979) 341-349.

[95] M. Ammiche, A. Kouadri. Constant false alarms rate for fault detection. 5th international conference on Electrical Engineering-Boumerdes (ICEE-B) (2017), doi:10.110.9/ICEE-B.2017.8191980.

[96] M. Ammiche, A. Kouadri, A. Bakdi. A combined monitoring scheme with fuzzy logic filter for plant-wide Tennessee Eastman Process fault detection. Chemical Engineering Science 187 (2018) 269–279.

[97] M. Ammiche, A. Kouadri, A. Bensmail. Fault detection and identification in a cement rotary kiln via adaptive thresholds and filtered monitoring indices. Unpublished paper.

[98] M. Ammiche, A. Kouadri, L.M. Halabi, A. Guichi, S. Mekhilef.. Fault detection in a grid-connected photovoltaic system using adaptive thresholding method. Solar Energy 174 (2018) 762–769.

[99] M. Ammiche, A. Kouadri, A. Bakdi. Adaptive thresholds monitoring scheme for fault detection in plant-wide industrial processes. Unpublished paper.

[100] M. Ammiche, A. Kouadri, A. Bensmail, A Modified moving window dynamic PCA with fuzzy logic filter and application to fault detection, Chemometrics and Intelligent Laboratory Systems (2018), doi: 10.1016/j.chemolab.2018.04.012.

[101] J. Ferahtia, N. Djarfour, K. Baddari, A. Kheldoun. A fuzzy logic-based filter for the removal of spike noise fom 2D electrical resistivity data. Journal of Applied Geophysics. 87 (2012) 19-27.

[102] D. Naso ,A. Scalera, G. Aurisicchio, B. Turchiano. Removing Spike Noise From Railway Geometry Measures With a Fuzzy Filter. Trans. Syst., Man, Cybern. Syst. 36 (2006) 485-494.

[103] M. Ammiche, A. Kouadri. False alarms rate reduction using filtered monitoring indices. Algerian Journal of Signals and System. 2 (2017) 40-50.

[104] A. Hamdouche, A. Kouadri, A. Bensmail, Kernelized relative entropy for direct fault detection in industerial rotary kilns, Int J Adapt Control Signal Process (2018) 1-13.

[105] J. J. Downs, E. F. Vogel. A plant-wide industrial process problem control. Computers & Chem. Eng. 17(1993)245-255.

[106] M. Kano, S.i Hasebe , I. Hashimoto, H. Ohno.. Statistical Process Monitoring Based on Dissimilarity of Process Data. AIChE Journal.48 (2002) 1231-1240.

[107] M. R. Maurya, R. Rengaswamy, V. Venkatasubramanian. Fault diagnosis using dynamic trend analysis: A review and recent developments. Engineering Applications of Artificial Intelligence. 20 (2007) 133-146.

[108] Q. Jiang. X. Yan. Nonlinear plant-wide process monitoring using MI-spectral clustering and Bayesian inference-based multiblock KPCA. Journal of Process Control, 32 (2015) 38–50.

[109] Z. Ge, F. Gao, Z. Song. Two-dimensional Bayesian monitoring method for nonlinear multimode processes. Chemical Engineering Science. 66 (2011) 5173–5183.

[110] L. Zhou, J. Chen, Z. Song, Z. Ge, A. Miao. Probabilistic latent variable regression model for process-quality monitoring. Chemical Engineering Science. 116 (2014) 296-305.

[111] Q. Jiang, X. Yan. Chemical processes monitoring based on weighted principal component analysis and its application. Chemometrics and Intelligent Laboratory Systems. 119 (2012) 11–20.

[112] M. Grbovic, W. Li, N. A. Subrahmanya, A. K. Usadi, S. Vucetic. Cold start approach for data driven fault detection. IEEE Trans. Ind. Informat. 9 (2013) 2264–2273.

[113] L. Jiang, Z. Song, Z. Ge, J. Chen. Robust self-supervised model and its application for fault detection. Ind. Eng. Chem. Res. doi: 10.1021/acs.iecr.7b00949.

[114] L. Luo, S. Bao, J. Mao, D. Tang. Fault detection and diagnosis based on sparse PCA and two-level contribution plots. Ind. Eng. Chem. Res. doi: 10.1021/acs.iecr.6b01500.

[115] A. Bathelt, N. L. Ricker, and M. Jelali. Revision of the Tennessee Eastman Process Model. IFAC-Papers OnLine. 48 (2015) 309-314.

[116] R. Hasan. S. Mekhilef. Highly efficient flyback microinverter for grid-connected rooftop PV system. Solar Energy. 146(2017) 511–522.

[117] M. Hossain, S. Mekhilef, M. Danesh, L. Olatomiwa, S. Shamshirband. Application of extreme learning machine for short term output power forecasting of three grid-connected PV systems. Journal of Cleaner Production. 167 (2017) 395-405.

[118] J. Wang, B. Zhong, J. Zhou, Quality-Relevant Fault Monitoring Based on Locality Preserving Partial Least Squares Statistical Models, Ind. Eng. Chem. Res. 56 (2017) 7009-7020.

[119] L. Ciabattoni, F. Ferracuti, A. Freddi, G. Ippoliti, S. Longhi, A. Monteriù. Fault detection of nonlinear processes based on switching linear regression models. IECON 42nd Annual Conference of the IEEE Industrial Electronics Society. (2016) 400-405, Florence, Italy.